USING SPECTRAL ANALYSIS TECHNIQUES TO IDENTIFY CHARACTERISTIC SCALES IN DIGITAL ELEVATION MODELS

A Thesis

by

ERIC JOSEPH GUENTHER

Submitted to the Office of Graduate and Professional Studies of
Texas A&M University
in partial fulfillment of the requirements for the degree of

MASTER OF SCIENCE

Chair of Committee,	Anthony Filippi
Co-Chair of Committee,	Burak Güneralp
Committee Members,	İnci Güneralp
	Matthias Katzfuß
Head of Department,	David Cairns

August 2017

Major Subject: Geography

ABSTRACT

Meandering river floodplains exhibit periodic structures which can be seen in features such as meander bends, point bars, and oxbow lakes. To improve our understanding and better analyze floodplain landscapes created by the dynamics of meandering rivers, characteristic scales need to be identified. Although methods that involve manual measurements of certain floodplain features are of utility, they are limited in their application and are typically very time intensive. Spectral analysis techniques represent an improved approach. For this research, two separate 2D spectral analysis techniques were used: the Fourier transform and the continuous wavelet transform. By using an appropriate theoretical red-noise background spectrum for the landscape, the spectral analysis techniques could provide a power spectrum which is then used to clearly identify the global and local characteristic scales. The results from the analysis of synthetic test images demonstrated such capability of both methodologies, and indicated that both performed similarly although the wavelet transform provides spatial information in addition to scale. The methodologies were then applied to simulated meandering river floodplain of meandering river where two ranges of characteristic scales were identified that corresponded to bend-scale and meander-train scale features. The characteristic meander-scale features also correlated with the surface metrics focal mean, the average elevation within a given area, and rugosity, the ratio between surface area of a given area and the surface area of a completely flat surface. The results show that the spectral analysis techniques can

identify characteristic scale of a meander-river floodplain and that the relationship to the surface metrics indicate that it provides information to the topographic structure of the floodplain.

DEDICATION

This work is dedicated in memory of Harry P. Dalton and Norman G. Guenther for providing the inspiration and support when I was a child that has driven me to reach this goal.

ACKNOWLEDGEMENTS

I would like to thank my committee chair, Dr. Anthony Filippi, my co-committee chair, Dr. Burak Güneralp, my committee members, Dr. İnci Güneralp and Dr. Matthias Katzfuß, and everyone in the Fluvial-Geoscience Group, especially Billy Hales and Cesar Castillo for their guidance, support, and camaraderie throughout the course of this research.

Thanks also go to friends and colleagues, the Department of Geography faculty and staff, Dudley's Draw, and especially my girlfriend, Hannah, for never leaving my side during my time at Texas A&M University.

Finally, I would like to thank those who mean the most to me: my mother, father, brothers, John and Stephen, and my grandparents, Grammy and Grampy, and Angel and Grandpa. Without their continuous and unrelenting encouragement and support this would not have been possible.

CONTRIBUTORS AND FUNDING SOURCES

Contributors

This work was supervised by a thesis committee consisting of Professor Anthony Fillipi as advisor, Professor Burak Güneralp as co-advisor, and Professor İnci Güneralp of the Department of Geography, and Professor Matthias Katzfuß of the Department of Statistics.

Much of the analysis on meandering-river floodplains was provided by Professor İnci Güneralp. The Matlab code used in this thesis was originally published by Professor Taylor Perron of Massachuettes Institute of Technology in the Department of Geology, Geochemistry and Geobiology and was modified by the student under fair use of the GNU General Public License given by the originally creator. All other work conducted for the thesis was completed by the student independently.

Funding Sources

There are no outside funding contributions to acknowledge related to the research and compilation of this document.

NOMENCLATURE

CWT	Continuous Wavelet Transform
DEM	Digital Elevation Model
DFT	Discrete Fourier Transform
DWT	Discrete Wavelet Transform
FWHM	Full-width at half-maximum
Wc	Width of river channel

TABLE OF CONTENTS

Page

LIST OF FIGURES

Page

LIST OF TABLES

Page

CHAPTER I

INTRODUCTION AND BACKGROUND

1.1 Introduction

The research in this thesis aims to develop a methodology to determine the characteristic scale of meandering river floodplain. Specifically, thesis will (1) develop a two-dimensional theoretical red noise model to test for significance (2) examine the characteristic scale of a meandering river floodplain using two different two-dimensional spectral analysis techniques: (a) discrete Fourier analysis and (b) discretized continuous wavelet analysis; and (3) compare the differences between these techniques using synthetically generated meandering river floodplains.

1.2 Background on frequency analysis of meandering rivers

Meandering rivers are periodic in shape and structure, which has attracted much research from fluvial geomorphologists for a long time (Winslow 1893, Davis 1905, Davis 1913, Baschin 1916). In particular, geomorphologists have sought ways of classifying the periodic nature of meandering rivers (Brown, Pasternack and Wallender 2014, Catano-Lopera, Abad and Garcia 2009, Zolezzi and Güneralp 2016, Abad and Garcia 2009). Applying signal-analysis techniques to a meandering river planform has shown that there are certain scales or frequencies which are characteristic or unique for a particular meandering river (Zolezzi and Güneralp 2016, Abad and Garcia 2009).

Geomorphologists have been interested in quantifying the periodic nature of meandering river floodplains to better understand and compare the fluvial processes that are occurring in different meandering river systems. Meandering rivers exhibit this

periodic nature at a range of scales, which can be seen in repeating meander bends or larger oscillations in the floodplain itself (Güneralp and Martson 2012). Meandering rivers cut and erode sediment to form outer banks, and transport eroded sediment downriver and to deposit it on the inner banks (Güneralp and Martson 2012). These processes shape a meandering river, depending on several factors such as the soil type and flow rate (Leopold, Wolman and Miller 1995), and depending on the age of the river, will shape the river floodplain in different ways (Leopold et al. 1995, Howard 1996). The processes that shape meandering rivers also shape the geomorphic forms commonly present throughout meandering river floodplains through the creation of pointbars, sleuths, and other mesoform such as floodplain massifs and meander scars (Leopold et al. 1995, Bedient and Huber 2002, Güneralp and Martson 2012).

A floodplain is an area from the banks of a river to the extent of a bounding valley or the area around a river which is inundated during a floodstage (Leopold et al. 1995, Bedient and Huber 2002). For a meandering river floodplain, the river itself is the largest geomorphic agent on the landscape and the primary creator of topographic features (Leopold et al. 1995, Bedient and Huber 2002). Meandering river floodplains may also contain areas, or geomorphic forms that indicate that a meander once existed such as meander scars and oxbow lakes (Leopold et al. 1995, Bedient and Huber 2002).

Transportation and deposition of sediments are primary geomorphic processes in forming the periodic geomorphic forms found in meandering river floodplains; upon visual inspection, major forms are located at almost predictable frequencies (Speight 1965). Studying the spatial and scale characteristics of the periodic geomorphic forms

within a meandering floodplain as well as of meandering rivers, can help further our understanding of the process-form relationships governing the evolution of these landscapes.

A large body of research has studied the scale-invariant or fractal nature of meandering river systems, meaning that the same periodic feature can appear at multiple scales (Nikora 1991, Stolum 1996). This, along with other research, seem to suggest that topographical features that are created through fluvial processes in a meandering floodplain are dominated by fractal structures. However, further research has shown that whereas landscapes may generally exhibit these characteristics, they are not fractal in a complete sense (Gilbert 1909, Mark and Aronson 1984, Gilbert 1989). Some of the past research into the periodic features of meandering river systems have indeed shown that certain scales or frequencies are more characteristic or unique for a particular river system. It is possible that identifying these scales which are characteristic of a certain river floodplain could serve as a sort of geomorphic "fingerprint." Then, this geomorphic fingerprint could be used to compare it to those of other meandering river floodplains. Thus, it can serve as a quantitative, analytical procedure for comparing differences in topographic structure which are qualitatively recognizable by geomorphologists.

1.2.1 Measuring Scales in a Landscape

Geomorphologists have long recognized periodic scales and features for meandering river systems (Labarbera and Rosso 1989, Crave and Davy 1997, Dodds and Rothman 2001) as well as in a variety of other landscapes and landscape features (Balmino 1993, Ahnert 1984, Hovius 1996, Dodds and Rothman 2000, Gilbert 1909).

Qualitative assessments of features of various periodic scales have been conducted since the mid- to late-1800s, including many pioneers in the field of geomorphology, such as G.K. Gilbert (1909) and W.M. Davis (1905). Whereas qualitative assessments of periodic features in landscapes have been performed for a long period of time, numerical assessment of scale within landscapes is a relatively more recent phenomenon. Many of these studies have exploited the fractal nature found in many landscapes to assess the scales found in a landscape (Mandelbrot 1975, Turcotte 1987, Newman and Turcotte 1990). However, determining characteristic scales in a landscape without using fractals as a basis is typically challenging. Landscapes that have parallel features with spacing can be easily inferred (Hovius 1996, Talling et al. 1997) although this can only be done in areas with simple, and clearly periodic, features.

Even identifying the frequency or scale of meandering river areas can be difficult through direct measurements of these areas (Horton 1932). Advances in spectral analysis have proven to be an effective way to measure scales and frequencies in a landscape. Spectral-analysis techniques, such as the Fourier transform, have been used throughout geomorphology and natural sciences to decompose a natural signal into the sinusoidal components which comprise the complete signal. Many studies have used Fourier analysis to better understand natural features both in the time (one-dimensional) and spatial (two-dimensional) domains (Gallant and Hutchinson 1997, Orloff, Kreslavsky and Asphaug 2013, Tary et al. 2014). Fourier analysis has proven to be effective in understanding frequency of features and understanding a landscape in terms of scale.

Perron, Kirchner, and Dietrich (2008) in particular, use Fourier analysis to identify characteristic scale in drainage landscapes by comparing the scale of a particular landscape to a theoretical purely fractal landscape. Scales which were significantly different from a theoretical pure fractal landscape could be considered to be characteristic. Perron et al.'s (2008) is the first, and thus far the only, to our knowledge, established technique for identifying landscape characteristic scales.

1.3 Research Gap in Determining Characteristic Scale of Meandering rivers

Perron et al. (2008) established a critical methodology for identifying characteristic scale in the landscape using the Fourier transform. However, there are a few areas of this methodology that could be improved to better identify characteristic scales within a riverine/fluvial landscape environment. For instance, Perron et al. (2008) use a theoretical fractal surface to establish their null hypothesis. Their null hypothesis could simply be written as:

The spectral power of a given scale for a landscape is the same of a similar theoretical fractal surface.

However, although there is much research pointing to landscapes being very similar to fractal surfaces (Mandelbrot 1975, Matsushita and Ouchi 1989), there is still considerable discord among geomorphologists, and fluvial geomorphologists in particular, who are skeptical of this claim (Horton 1945, Ijjaszvasquez, Rodriguez-Iturbe and Bras 1992, Valenzuela, Lins and De Oliveira 2013). Thus, using a theoretical fractal surface as the basis for null hypothesis generation for areas that are not considered to

have a baseline fractal nature would not result in characteristic scales that are acceptable. Therefore, another baseline must be used to establish a null hypothesis in this context.

One potentially useful concept within the geosciences, including geomorphology and meteorology, is the concept of a theoretical red noise. Theoretical red noise has been commonly used for null hypotheses for geoscience applications (Caswell and Cohen 1995, Meyers 2012). Red noise exhibits increases in spectral power as the frequency decreases, as opposed to white noise, where spectral power remains relatively constant throughout all frequencies (Gilman, Fuglister and Mitchell 1963, Montgomery and Dietrich 1992). In a sense, using a theoretical fractal could be considered a type of theoretical red noise, though the difference would be that a theoretical fractal would be scale-invariant. Theoretical red noise, on the other hand, is based on an autoregressive-1 (AR-1) model (Gilman et al. 1963, Meyers 2012, Torrence and Compo 1998). The result is a baseline which does not rely on the assumption that a default landscape would be a pure fractal. The null hypothesis in this situation would be:

The spectral power of a given scale for a landscape is the same of a similar theoretical red-noise surface.

To our knowledge, there is no previous research that employs a two-dimensional red-noise model in order to establish a null hypothesis which is then used to identify characteristic scales within a landscape. A null hypothesis such as this would be free from the restrictive assumption of a fractal baseline and allow for a wider variety of applications, so long as they generally exhibit some sort of baseline similar to a red (or pink, white, etc.) model.

In addition, whereas the Fourier transform is perhaps the most commonly-used spectral-analysis technique for geosciences applications and is very robust, it does have shortcomings. For example, although the Fourier transform is able to decompose a signal into its sinusoidal components, it loses the temporal or spatial information associated with these components by taking the components into the frequency domain. Whereas orientation is preserved in a two-dimensional Fourier transform, the spatial information is lost (Kaiser 1994). In addition, the Fourier transform is unable to process non-stationary signals properly, which are commonly found in nature and geoscience applications (Sayles and Thomas 1978, Massel 2001).

To address these issues, the wavelet transform will be used in the present research. While other works have used 2D wavelet analysis to understand different characterstisics of landscapes, such as Booth et al. (2009), which used wavelets to study areas that are more prone to landscapes, there has not been any works to our knowledge that have used 2D wavelet analysis to identify characteristics scales. Wavelet analysis decomposes a signal into different scale components. Two advantages it has over the Fourier transform are that it is able to preserve temporal and spatial information within the wavelet coefficients (Kaiser 1994); and that it is able to process non-stationary signals found in nature (Kaiser 1994, Massel 2001, Labat, Ronchail and Guyot 2005). These benefits warrant further investigation into the effectiveness of using the wavelet transform to serve as the spectral-analysis component in identifying characteristic scale of a landscape.

1.4 Research Objectives

The purpose of this research is to identify the characteristic scales of a meandering river floodplain. This will be accomplished by achieving two objectives:

1. Develop a two-dimensional theoretical background spectrum model to be able to test for significance.
2. Identify the characteristic scales of a meandering floodplain using two-dimensional spectral-analysis techniques: (a) discrete Fourier analysis and (b) discretized continuous wavelet analysis.
3. Compare the differences in performance between these techniques for synthetic digital elevation models (DEMs).

1.5 Mathematical Background

1.5.1 Fourier Analysis

The Fourier transform is able to decompose a signal into the sinusoidal components of the complete signal. The Discrete Fourier transform (DFT) is able to convert a finite series of samples into a list of coefficients which represents a finite combination of these sinusoidal frequencies. The Fourier transformation for a time-series is defined as (Kumar and Foufoula-Georgiou 1997):

$$\hat{f}(\omega) = \int_{-\infty}^{\infty} f(x) e^{-2\pi i \omega x} dx \qquad \text{I-1}$$

where x represents a time series and ω represents the angular frequency given in Hertz. Although developed initially to analyze 1D signals, it can be extended to accommodate a

2D signal, or image. Through using the DFT on an image, the frequency components and their orientation can be identified in a 2D frequency space. Computing the Fourier coefficients for an image can be accomplished using the 2D Fourier transform as follows (Kumar and Foufoula-Georgiou 1997):

$$\hat{f}(\omega_x, \omega_y) = \int \int_{-\infty}^{\infty} f(x,y) e^{-2\pi i(\omega_x x + \omega_y y)} dx dy \qquad \text{I-2}$$

where x and y represent the horizontal and vertical components in space, respectively and ω_x and ω_y represent the angular frequency for the x and y components, respectively. Typically when dealing with two-dimensional arrays in a conventional computer system, the two-dimensional discrete Fourier transform can be used. The two-dimensional DFT is given by (Booth et al. 2009):

$$\hat{f}(k_x, k_y) = \sum_{m=0}^{N_x-1} \sum_{n=0}^{N_x-1} f(m\Delta x, n\Delta y) e^{-2\pi i(\frac{k_x m}{Nx} + \frac{k_y n}{N_y})} \qquad \text{I-3}$$

where k_x and k_y are the wavenumbers in the x and y direction, and m and n are the indices in the f array. N_x and N_y represent the total number of elements in the x and y directions. The resulting Fourier coefficients are commuted into 2D frequency space in which the orientation of frequency components are held, though the spatial relationships within the

image are not preserved in the frequency domain. The DFT is not able to accurately measure non-stationary signals, which is a signal that has a frequency that changes throughout space or time. It has been observed that non-stationary signals are common in natural areas (Sayles and Thomas 1978, Massel 2001). Accounting for non-stationary frequencies has not been fully addressed in studying characteristic scale in previous 2D studies, though it has been very effective in extracting periodic features in landscapes (Torrence and Compo 1998, Kaiser 1994).

1.5.2 Wavelet Analysis

Similar to the Fourier transform, the wavelet transform is able to decompose a complex signal into its individual wavelet components. Instead of decomposing the signal into sinusoidal components, however, the continuous wavelet transform decomposes a signal into wavelets, which is a wave that oscillates from zero to a non-zero value, and back to zero (Addisson 2004). The wavelet transform can be performed on 1D signals and 2D images and is able to preserve time/location information content of the original data (Antonie et al. 2004) . As a result, the wavelet coefficients produced through a wavelet transform contain a "time-frequency" representation of the data which allows for time and frequency localization (Addisson 2004, Bruun and Nilsen 2003, Yoo 2001). This allows wavelet coefficients to indicate the frequency components at a specific time or location. In addition, wavelets are able to accurately capture frequencies which are non-stationary (Addisson 2004). As natural signals and landscapes often contain non-stationary signals, this makes using wavelet transforms seem to be desirable (Weedon 2003).

For this research, we are primarily focused on utilizing the 2D variant of this transform. There are two major varieties of the wavelet transform—the Discrete Wavelet Transform (DWT) and the Continuous Wavelet Transform (CWT) (Labat 2005). The discrete wavelet transform operates as a filter bank, decomposing a signal into detail and approximation coefficients for each dyadic scale (Addisson 2004). The continuous wavelet transform is able to calculate wavelet coefficients for all possible scales; however, many of these scales may contain redundant information (Addisson 2004, Mount et al. 2013, Yoo 2001). Because we are interested in measuring characteristic scale—not just at dyadic scales, but across all possible scales—the continuous wavelet transform will be used. In addition, the continuous wavelet transform will be able to capture signals isotopically. Although there are directionalities in the fluvial landscape/river floodplain in which we will be particularly geomorphically interested, we will initially use the CWT to identify characteristic scales in the landscape.

There are several reasons for using the 2D CWT instead of the 2D DWT in this context. Despite the 2D DWT being faster with respect to computation time, it entails some limitations that, for this research, makes CWT more useful. The primary limitation is that the DWT only operates at dyadic scales (Addisson 2004). Whereas most of the information resides in these scales, the DWT is unable to measure differences in coefficients between these scales easily. When considering mesoform landscape features, there is a large difference between a feature that is 32 meters in dimension versus a feature that is 64 meters in dimension, for example. It is crucial that

the CWT be able to operate between these scales when differentiation between/among features is needed. In addition, the CWT provides information to the scale at which it will be most comparable to the DFT versus the DWT. DFT is able to measure frequencies which can be converted to wavelengths at a variety of wavelengths, using the DWT only for scales which were dyadic. Therefore, the CWT would serve as a better analogue to compare the results to the DFT. If we are given that (Yoo 2001):

$$f(x) \in L_2(\mathbb{R})_2 \qquad \text{I-4}$$

or that a time-series in which all values in the time-series are real values, then the wavelet coefficients can be computed by (Kumar and Foufoula-Georgiou 1997):

$$\text{cwt}(s,b) = \frac{1}{\sqrt{s}} \int f(x)\psi(\frac{x-b}{s})dx \qquad \text{I-5}$$

in which *s* represents a particular wavelet scale, and *b* represents a specific location in the time-series. The wavelet coefficients may also be computed in the Fourier-dimension, which results in faster computation. A one-dimensional time-series can be computed using:

$$\text{CWT}(s,\omega) = \sqrt{s}\,\hat{f}(x)\,\hat{\psi}(s\omega) \qquad \text{I-6}$$

where ω is the Fourier component of the time-series. Like the Fourier transform, the wavelet transform can also be used for two-dimensional series. Similar to the time-

series, given a two-dimensional series in which all values in the time series are real values, or (Yoo 2001):

$$f(x,y) \in L_2(\mathbb{R})_2 \qquad \text{I-7}$$

then the wavelet coefficients can be computed from the two-dimensional series using (Booth et al. 2009):

$$\mathrm{C}(s,a,b) = \frac{1}{s}\iint f(x,y)\psi(\frac{x-a}{s},\frac{y-b}{s})\,dxdy \qquad \text{I-8}$$

where *a* and *b* both represent a location in the time domain, and where ψ is a particular wavelet. For a Mexican Hat wavelet, the wavelet is defined as (Booth et al. 2009):

$$\psi(x,u) = (x^2+y^2-2)e^{-\frac{1}{2}(x^2+y^2)} \qquad \text{I-9}$$

Similar to the one-dimensional variation of the wavelet transform, the 2D CWT can also be computed in the Fourier domain, allowing for more computationally-efficient calculations of the wavelet coefficients. For this, the wavelet transform is defined as (Yoo 2001):

$$\mathrm{CWT}(s,\omega_1,\omega_2) = s\,\widehat{f}(\omega_1\omega_2)\,\hat{\psi}(s\omega_1,s\omega_2) \qquad \text{I-10}$$

and the Mexican Hat wavelet being defined as (Yoo 2001):

$$\hat{\psi}(\omega_1,\omega_2) = -2\pi(\omega_1^2+\omega_2^2)e^{-\frac{1}{2}(\omega_1^2+\omega_2^2)} \qquad \text{I-11}$$

The Mexican Hat wavelet, also known as the Marr wavelet, is a wavelet composed of a negative normalized second derivative of a Gaussian function (Torrence and Compo

1998). The wavelet itself is isotropic and radially symmetrical, which are properties that will be particularly useful for studying radial features exhibited in meandering floodplains, such as point bars, etc. While the river which shapes a meandering river floodplain has an inherent directionality interpreted as a single unit, it through the creation of meanders, the direction of flow can be in multiple orientations along any point of a river. The Mexican Hat wavelet in the spatial domain can be seen in Figure 1.

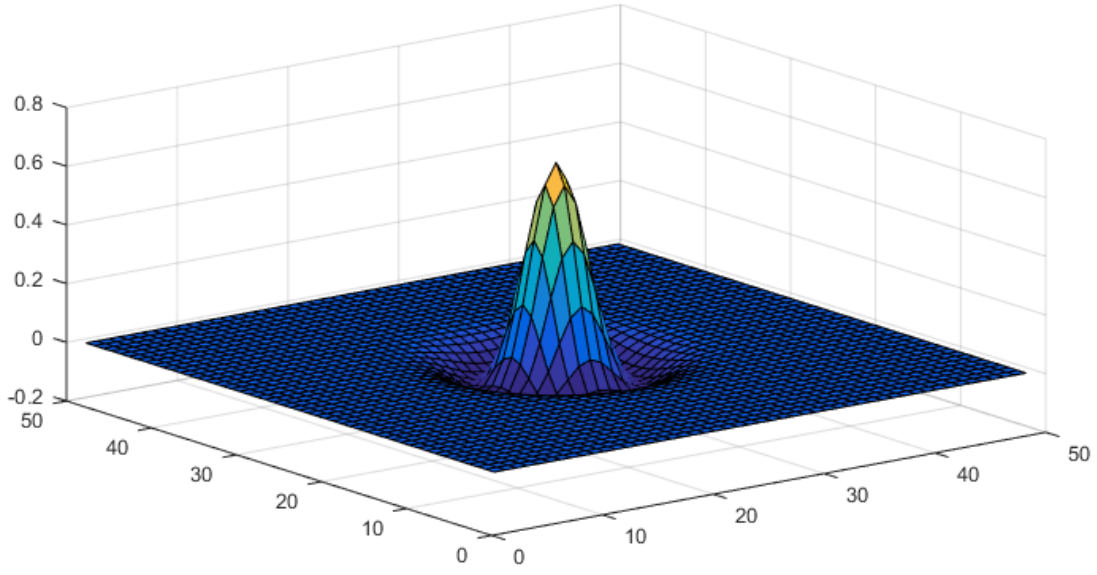

Figure 1. Example of Mexican Hat wavelet in the spatial domain.

1.5.3 Power Spectrum

Once Fourier and wavelet coefficients have been computed from the data, the question becomes how to best interpret these values. One common method of interpretation is based on examination of the power spectra. The power spectra answer the question of how much each scale or frequency contributes to the overall signal. The

power spectra for a Fourier transform can be modeled using (Torrence and Compo 1998):

$$V_{DFT} = \frac{1}{N_x^2 N_y^2} \left| Z(k_x, k_y) \right|^2 \qquad \text{I-12}$$

Similarly, the power spectra can be computed from the wavelet coefficients using this equation (Torrence and Compo 1998):

$$V_{CWT} = \frac{1}{2N_a^2 N_b^2} |C(s, a, b)|^2 \qquad \text{I-13}$$

In the case of wavelets, the power spectra can also provide information regarding where in space or time a particular scale contributes to an overall signal. From this, the main components of a signal or image can be assessed. In the case of DEMs, the power spectra informs on what aspects of the landscape contributes most to the overall landscape. In essence, the power spectra constitute a measure of the amplitude of a particular signal.

1.5.4 Justification for background spectrum

To answer the question "*What is the characteristic frequency or scale of a landscape?"* the most basic definition of the characteristic feature of a particular landscape could perhaps be the frequency or scale with the highest power spectra. However, this is not an entirely accurate representation of characteristic scale. Because power spectra essentially constitute a measure of signal amplitude, high-amplitude features would always be considered characteristic in a particular landscape. However,

in natural signals and landscapes, low-frequency or large-scale features typically have the highest amplitude. Because of this, the power spectra of natural signals and landscapes will almost always be biased towards the low-frequency components. The characteristic frequency or scale, in simplest terms, is an aspect of the landscape that deviates from a theoretical norm (Torrence and Compo 1998) In order to accurately identify characteristic scale, a background spectrum must be compared to the power spectrum calculated from the landscape in order to identify characteristic scale (Torrence and Compo 1998).

1.5.4.1 Background Spectrum: Binned Values

The simplest method of calculating a background spectrum is to compute the average values of the spectra at each scale or for a certain range of frequency components. The line of best fit between these binned averages can be used as an initial approach to establishing a background spectrum. This method was mentioned as a possibility by Perron et al. (2008), and it does serve as approximation and is easy to compute. However, the background spectrum computed from binned values would be biased towards areas with high spectral power.

1.5.4.2 Background Spectrum: Theoretical Fractal Values

If a landscape can be considered to be a fractal surface, then it could be used to generate a background spectrum, which can be used to identify characteristic scales or frequencies, or scales and frequencies which deviate from an expected fractal. One method for calculating the theoretical background spectrum using a theoretical fractal is to generate a large quantity of simulated fractal surfaces that have similar variance and

range parameter values to the target landscape (Perron, Kirchner, and Dietrich 2008). There are several algorithms which can be used to simulate a fractal landscape; one of the most commonly used such methods is the diamond-square algorithm (Fournier, Fussell and Carpenter 1982). Perron et al. (2008) generated 1,000 fractal surfaces of similar range and variance value to the landscape of interest, and they averaged the spectral power of these fractal surfaces to generate a background power spectrum that represents the power spectrum of a theoretical fractal surface. This methodology for developing a background spectrum is effective; however, its main weakness is that the null hypothesis for determining characteristic scale or frequency would be that the landscape is a fractal. This essentially assumes that most landscapes are inherently fractal. However, there is much debate as to whether landscapes can truly be thought of as fractals (Gilbert 1989, Meyers 2012, Zolezzi and Güneralp 2016). As a result, such a methodology for developing the background spectrum does not provide a good null hypothesis for the present research.

1.5.4.3 Background Spectrum: Mathematical Theoretical Red Noise for Time Series in 1D

A more accurate depiction of background spectrum is to create theoretical red noise using data derived from the original data in interest(Meyers 2012). If white noise is noise that occurs at all frequencies, red noise is noise which exhibits larger amplitudes at low frequencies (Gilman et al. 1963, Mitchell 1964). Similarly, natural signals and landscapes tend to have larger amplitudes at longer wavelengths (i.e., at lower frequencies) than at short wavelengths (Gilman et al. 1963, Torrence and Compo 1998).

Because of this, computing and the equivalent theoretical red noise spectrum could be used as a theoretical background spectrum to identify characteristic scales. The term "red noise" was first used in the literature regarding analysis of spectral power by Ward and Sharpiro (1961), who qualitatively described how time series of metrological and natural signals have power spectrum, which at high frequencies has high autocorrelation between successive measurements and that suppresses the variance, and also has inflation at lower frequencies. Such characteristics are in contrast to white noise, which has an even distribution of variance across all frequencies. The amount of "redness" that a theoretical background red noise has depends on the degree of autocorrelation that is exhibited by a signal. Autocorrelation values which are low will exhibit a higher degree of "redness." A red noise system can be modeled in 1D as follows (Gilman et al. 1963):

$$x_n = \alpha x_{n-1} + z_n \qquad \text{I-14}$$

where x_n represents a time series at location n with $x_0 = 0$, z_n is Gaussian white noise, and α is the assumed lag-1 autocorrelation. For a particular time-series that is normalized by subtracting-off the mean and dividing by the standard deviation, α can be determined by (Southworth 1960):

$$\alpha = \frac{\sum x_n x_{n+p}}{\sum x_n^2} \quad n = 1 \; to \; N - p \qquad \text{I-15}$$

where N is the total number of observations in a time-series, and p is the lag between observations. We also assume a constant standard deviation, independent of the range of

the summation. If we also consider the time-series with a mean value equal to zero we can determine the autocovariance function *W(p)* as (Southworth 1960):

$$W(p) = \frac{1}{N-p}\sum_{n=1}^{N-p} x_n x_{n+p} \qquad \text{I-16}$$

Then it can also be said that (Southworth 1960):

$$\alpha = \frac{W(p)}{\sum x_{n+p}^2} \qquad \text{I-17}$$

For a continuous time-series function represented by x(t), the autocovariance function *W(p)* can be represented as (Southworth 1960):

$$W(p) = \lim_{T\to\infty} \frac{1}{T}\int_{-T/2}^{T/2} x(t)x(t+p)\,dt \qquad \text{I-18}$$

Blackman and Tukey (1958) later showed that this is related to a Fourier transform of the power distribution function *P(f)* as (Southworth 1960):

$$W(p) = \int_{-\infty}^{\infty} e^{i2\pi fp} P(f)\,df \qquad \text{I-19}$$

where *P(f)* is expressed as (Southworth 1960):

$$P(f) = \lim_{T\to\infty}\left[\int_{-\infty}^{\infty} x(t)e^{i2\pi fp}\,dt\right]^2 \qquad \text{I-20}$$

Because autocovariance function *W(p)* is the Fourier transform of *P(f)*, *P(f)* can also be expressed as (Southworth 1960):

$$P(f) = \int_{-\infty}^{\infty} W(p) e^{-i2\pi fp}\, dp \qquad \text{I-21}$$

The relationship between the autocovariance function and the power spectrum of a real time-series that is symmetric around $p = 0$, $W(p)$ and $P(f)$ may be expressed as a two-sided cosine transform as follows (Southworth 1960):

$$W(p) = 2\int_{0}^{\infty} P(f) \cos 2\pi fp\ \, df \qquad \text{I-22}$$

$$P(f) = 2\int_{0}^{\infty} W(p) \cos 2\pi fp\ \, dp \qquad \text{I-23}$$

When the time-series $x(t)$ is a discrete time-series, then a discrete Fourier transform is needed. When a spectrum involves angular frequencies no greater than π, raw estimates of the spectral density can be found by (Southworth 1960):

$$L_p = W_0 + 2\sum_{q=1}^{M} W_q cos\frac{qp\pi}{M} + W_M \cos(p\pi) \qquad \text{I-24}$$

This can be further simplified by treating the $W(p)$ values as if they were the autocorrelation coefficients, α; if so, we come up with (Southworth 1960):

$$L_p = 1 + 2\sum_{q=1}^{M} \alpha_q cos\frac{qp\pi}{M} + \alpha_M \cos(p\pi) \qquad \text{I-25}$$

An alpha-value is generated from the lag-1 and lag-2 autocorrelation values in which (Gilman et al. 1963):

$$\alpha = \frac{\alpha_{1+\sqrt{\alpha_2}}}{2} \qquad \text{I-26}$$

where α_1 is the lag-1 autocorrelation and α_2 is the lag-2 autocorrelation. Gilman et al. (1963) use this equation to model the theoretical red noise because of the relationship between autocorrelation and the "red noise." The equation can be further simplified to (Gilman et al. 1963):

$$P_k = \frac{1-\alpha^2}{1-2\alpha\cos\frac{2\pi k}{M}+\alpha^2} \qquad \text{I-27}$$

The P_k value returned by this equation will represent the theoretical background red noise, which contains higher power at lower frequencies and lower power at higher frequencies. If the system more closely resembles a white-noise system, then the theoretical background spectrum will be equal to 1 at all frequencies. The results from this methodology are directly comparable to the Fourier power spectrum of a one dimensional time-series that has been normalized by $N/2\sigma^2$. The theoretical background spectrum will be required for defining the null hypothesis for defining characteristic scale, with more information given on this in subsequent sections. The theoretical background red noise spectrum can also be used as the null hypothesis for wavelet; however, the Fourier periods are not inherently comparable to wavelet scale. As a result, the equivalent Fourier period for each wavelet scale needs to be determined.

1.5.4.4 Background Spectrum: Mathematical Red Noise for Time Series in 2D

The one-dimensional theoretical red noise spectrum provides a robust method that can be used to identify characteristic scale. Furthermore, many of the same concepts that serve as the basis for the one-dimensional theoretical red noise spectrum can be expanded to find a two-dimensional theoretical red noise spectrum for a two-dimensional series. Similar to Equation 19, the two-dimensional case for the 2D Fourier transform using Cartesian coordinates can be written as (Mack 2011):

$$P(f_x, f_y) = \int \int_{-\infty}^{\infty} G(x,y) e^{-i2\pi(f_x x + f_y y)} dx dy \qquad \text{I-28}$$

For the 2D Fourier transform using polar coordinates, the conversions (Mack 2011):

$$x = r\ cos\theta \qquad \text{I-29}$$

$$y = r\ sin\theta \qquad \text{I-30}$$

$$f_x = f_r\ cos\varphi \qquad \text{I-31}$$

$$f_y = f_r\ sin\varphi \qquad \text{I-32}$$

can be used for the 2D Fourier transform using polar coordinates as follows (Mack 2011):

$$P(f_r\varphi) = \int_0^{\infty} \int_0^{2\pi} G(r,\theta) e^{-i2\pi\, f_r r\, cos(\theta-\varphi)} r dr d\theta \qquad \text{I-33}$$

If it involves a radial symmetrical function, the Hankel transform can be used with the θ integration can be written as (Mack 2011):

$$P(f_r) = 2\pi \int_0^{\infty} r\, G(r)\, J_0(2\pi\, f_r r) dr d\theta \qquad \text{I-34}$$

where J_0 represents the Bessel-function of the first kind, zero order.

This conversion will be discretized in order to accommodate a finite two-dimensional series. The equivalent α value will be computed by using the autocorrelation lag-values that were derived using semi-variograms. The experimental semi-variogram of the target landscape will be generated from the target landscape itself. Next, a modeled semi-variogram will be generated using parameter values derived from the experimental semi-variogram. Next, the lag-1 and lag-2 values from the modeled semi-variogram will be used to find α, which will be used to determine the amount of "redness" in the landscape.

1.5.4.5 Numerical Approach to Generating Background Red Noise

Although there exists an analytical approach to calculating the theoretical background red noise spectra, a numerical approach also exists (Lennon 2000). While in the analytical the theoretical background red noise spectrum can be calculated from the autocovariance of the original data, for the numeric approach, the theoretical red noise background spectrum can also be calculated from the power spectrum of the original data. The equation is given as (Lennon 2000, Voss 1988):

$$P(f) \propto f^{\beta} \qquad \text{I-35}$$

Where P is the power spectrum at a particular frequency, f, and β is the degree of "redness." This relationship allows for β to be solved for using the equation:

$$\beta \propto \frac{\log 10^{P(f)}}{\log 10^{f}} \qquad \text{I-36}$$

Which can be used to calculate an approximate "redness" for a particular image based off of the image's power spectrum.

1.5.5 Equivalent Fourier Period for Wavelet Scales

Whereas the Fourier transform and wavelets essentially dissemble signals into their signal components, each wavelet scale cannot be directly related to its equivalent frequency as it can for each Fourier period. However, it has been shown that the relationship between an equivalent Fourier period and a wavelet scale can be found analytically (Torrence and Compo 1998, Booth et al. 2009). In simplest terms, the relationship can be found by fitting a cosine wave of a known frequency to a wavelet, and computing the scale that reaches the maximum value. The result is a ratio which can be used to find the equivalent wavelet scale for each Fourier scale. This can then be used to compare the theoretical background red noise spectrum to the power spectrum of the time-series in question.

Torrence and Compos (1998) has still provided several of the equations required to convert wavelet scale to an equivalent wavelength for several different wavelets, including the Mexican Hat wavelet, which for a 2D image would be:

$$w = \frac{2\pi x s}{\sqrt{\frac{5}{2}}} \qquad \text{I-37}$$

In which *w* is the wavelength, *x* is the sample size, and *s* is wavelet scale. This equation allows for easy comparison of wavelet and Fourier results which is crucial for comparing these two, as well as relating the scale sizes to wavelength sizes in the image.

1.5.6 Significant Testing: Inverse Chi Squared

Once a theoretical background spectrum is defined, a test of statistical significance will need to be implemented in order to determine whether the results are significant. As

mentioned previously, if the target landscape has a significantly higher spectral power than the theoretical background spectrum at a particular scale, then that scale could be considered characteristic. (Torrence and Compo 1998, Perron et al. 2008). Generally, the higher the spectral power of the target landscape is compared to the theoretical background spectrum, the more certain it is that the scale is representing a characteristic feature and not attributed to randomness. (Torrence and Compo 1998, Perron et al. 2008). An inverse chi-squared will be used to define a 95% confidence interval and identify characteristic scales (Torrence and Compo 1998, Perron et al. 2008). It is possible that even power spectra exceeding the 95% confidence interval may not be attributed to a true feature but attributed to randomness; therefore, frequencies or scale components that exceed this interval will need to be examined (Torrence and Compo 1998). Frequencies or scales that display some degree of clustering more likely represent a true feature that is statistically significant. The inverse chi-square equation can be used for identifying the characteristic scale or frequency. Given a background noise spectrum, the distribution of the Fourier power spectrum is (Torrence and Compo 1998):

$$\frac{N|\hat{x}_k|^2}{\sigma^2} \Rightarrow \frac{1}{2} P_k \chi_2^2 \qquad \text{I-38}$$

and for the wavelet power spectrum is (Torrence and Compo 1998):

$$\frac{|W_n(s)|^2}{\sigma^2} \Rightarrow \frac{1}{2} P_k \chi_2^2 \qquad \text{I-39}$$

where the "⇒" represents "is distributed as," and P_k is the mean background spectrum at Fourier frequency k that is equal to the wavelet scale s as determined by equivalent Fourier-period/wavelet scale.

This will serve as the basis for identifying significant results. Using the inverse chi-square and an appropriate theoretical red noise spectrum for a given image, features that have a spectral power above the 95% confidence interval can be considered significant.

1.6 Vital works done in spectral analysis of geophysical processes and landscapes

Several key publications in spectral analysis for geoscience applications and landscapes play a crucial role in shaping this study. Briefly, the following sections will detail how some of these publications that provided the foundation for this thesis and how they contributed to the field of spectral analysis in geomorphology.

1.6.1 Torrence and Compo's contribution to wavelet analysis

Torrence and Compo (1998) were certainly not the first to conceive the idea of characteristic scale, but their publication on identifying characteristic scales in wavelets have been cited (as well as their code libraries and packages that went along with their work used) so many times that their name has become ubiquitous to wavelet analysis in the geosciences. Much of the work done in this thesis seeks to mirror mimic much of what Torrence and Compo (1998) have done in spirit, though implement it two-

dimensionally as opposed to their work which is largely dealing with one-dimensional time- or spatial series.

In this work, they provide a justification of the differences and the advantages of wavelet analysis over using Fourier analysis, stating that the largest disadvantage of Fourier analysis is the inability to local a particular frequency in a time-series. They also bring up that even windowed Fourier analysis, which seeks to solve add the ability of localizing signals in a time-series by using various sizes of sliding windows and analyzing the results of each of the windowed results. However, they cite (Kaiser 1994, Torrence and Compo 1998) which state that the windowed Fourier transform is not accurate nor efficient in localizing frequencies in a time-series, and go on to cite the issue is from aliasing of frequency components which do not fall into the frequency range of particular window.

This sets up Torrence and Compos to introduce the wavelet transform, which they explain that a wavelet function is able to identify various scales in a signal, which could be compared to frequencies in a Fourier transform. They also show that wavelets are not limited by the same issues that the Fourier transform has with the ability of finding the location of various scales in a signal. In addition, because wavelets are able to identify the location of various scales along a time-series, they are then better able to handle non-stationary signals, which are not uncommon in natural signals.
Torrence and Compo then outline two ways a continuous wavelet can be calculated, one by performing a convolution to the original data using a wavelet at various scales, and a faster operation which requires a Fourier transform, but then a similar convolution of a

wavelet. Both results would still, however, yield the same results. Torrence and Compo later explain the differences between different types of wavelets including the difference between discrete (orthogonal) and continuous (nonorthongal) wavelets, the largest being the large amounts of data redundancy with continuous wavelets. However, for analyzing time-series of natural signals where smooth-transitions are more likely, the data redundancy may be useful. Though it is also important to note that this redundancy means that at certain scales, especially larger scales, the wavelet spectrum at adjacent scales will be highly correlated. Related to that, they emphasis the importance of selecting the right wavelet for a particular application. They differentiate between complex and real wavelets, with complex returning information about both amplitude and phase, which is perhaps better for capturing information about the oscillatory nature of a particular signal, versus real wavelets functions which return information at is better at identifying isolated peaks or discontinuities in a particular wavelet.

They also discuss how the "structure" of the wavelet can affect the results as well, and discuss selecting a wavelet with an appropriate width and shape. With wavelets, there is a trade-off of having better time accuracy or better frequency accuracy. Most wavelet functions strive to strike some sort of balance between the two, though different wavelet functions may be slightly better in one than the other. In addition, the shape of the wavelet function should mimic the property that is desired. A way wavelets can be thought of as is simply measuring how closely a waveform fits a signal. However, they state that if the primary interest is the wavelet power spectra, then the wavelet will not have a huge impact and will provide the same qualitative result.

While the wavelet results themselves are useful, they are not very useful by themselves. The wavelet power spectra answers the questions of which frequencies drive the overall signal. If the power spectra of a wavelet transform want to be interpreted in a way that is intuitive and useful, a baseline or theoretical background spectrum need to be computed. They note that most geophysical processes resemble either white or red noise processes, with white noise would be a random signal that has an autocorrelation value of 0 with red noise being a random signal that has an autocorrelation value greater than 0. They provide equations needed to find these values, and once a degree of noise is selected, the Fourier power spectra for that noise can be calculated, or a theoretical background spectrum sometimes referred to as a noise spectrum. An inverse-chi squared in conjunction with the theoretical background spectrum is used to establish confidence intervals. These confidence intervals indicate where the target spectrum is different than the theoretical background spectrum and could answer the question "where and what scales are in a time-series are characteristic or significant?" The establishment of a theoretical background spectrum is crucial in identifying scales that would be significant to a time-series. In much of the same way, this work will establish a background spectrum that will then be used to identify which scales are characteristic.

This has been crucial for geoscientist to understand time- and spatial-series and has led to many scientific discoveries. This research seeks to follow a similar outline in research, however, by allowing for two-dimensional analysis, this research seeks to be

able to conduct similar analysis on landscapes and digital elevation models, and not simply one-dimensional arrays.

1.6.2 Perron, Kirchner, and Dietrich's identifying characteristic scales using Fourier and fractals

Taylor Perron, James W. Kirchner, and William E. Dietrich (2008) published "Spectral signatures of characteristic spatial scales and nonfractral structures in the landscape" in which they find characteristic scales in the landscape in a very similar way that is sought after in this research. They start by citing that most landscape surfaces tend to follow a fractal relationship. By identifying scales which are do not conform to this fractal relationship, they could identify characteristic scales by their definition. In this publication, Perron et al. use a two-dimensional discrete Fourier transform as the basis for the algorithm. This work has a very similar a very similar methodological framework to Torrence and Compo (1998) despite Torrence and Compo utilizing a wavelet approach on one-dimensional signals. While Torrence and Compos (1998) define a characteristic scale as a particular scale that has a significantly higher spectral power than the theoretical background red noise, Perron et. al (2008) define characteristic scale as a particular scale that has a significantly higher spectral power versus the spectral power of a theoretical, yet comparable, purely fractal surface. They then use an inverse-chi square test similar to the one implemented in Torrence and Compos (1998) to identify scales which could be considered characteristic. When implementing this algorithm on high-resolution Lidar DEMs of ridge-valley areas, they were able to positively identify the characteristic scales.

While able to successfully identify characteristic scales, the algorithm and definition used to define a characteristic scale did present few shortcomings. For one: the definition for characteristic scale used by Perron et al. (2008) assumed that more landscapes follow a pattern that landscapes are in fact characteristic. However, there is much debate among geomorphologist which put this into doubt (Caswell and Cohen 1995, Meyers 2012). As a result, a more accurate definition for characteristic scale would be a scale in which the spectral power is significantly higher compared to a red noise background, which is the same approach used by Torrence and Compos (1998). In addition, this publication did not explore the use of wavelet analysis for this algorithm which has several advantages over the Fourier transform (Wang and Lu 2009). Implementing an algorithm that uses a theoretical background spectrum and also wavelet analysis may be able to produce results which can give better ideas exactly what the characteristic scales are within a landscape in addition to where these characteristic features exist within that landscape.

1.6.3 Booth, Roering, and Perron's work of studying landslides with wavelet analysis

"Automated landslide mapping using spectral analysis and high resolution topographic data: Puget Sound lowlands, Washington, and Portland Hills, Oregon" written by Adam M. Booth, Josh J. Roering, and Taylor Perron (2009) utilizes several of the ideas and concepts from "Spectral signatures of characteristic spatial scales and nonfractral structures in the landscape" by Perron et al. (2008). In this paper, they attempt to use spectral analysis to identify the location of areas that were at high risk for landslides using a high resolution Lidar DEM – as previous methods required manual

expert identification using either field studies or high resolution stereographic imagery. This work analyzed the power spectra of areas that were at higher risk to those areas that were at a lower risk of a landslide by comparing the power spectra of these areas, using both sliding window Fourier transform and wavelet analysis. When normalizing the power spectra of areas that were prone to landslides versus areas that are not prone to landslides, they were able to identify a range of scales which are associated with landscapes. Because wavelet analysis preserves the spatial information associated with different scales, the specific features or locations that contain the scales of interest can be easily identified. Typically, Fourier analysis is not capable of this, however, by using a sliding window Fourier transform, they were able to essentially perform a Fourier analysis which contains spatial information on where scales of interest are located, similar to the wavelet. While the differences were subtle, they concluded that the wavelet analysis proved more effective at this landslide analysis.

Similar to Perron et al. (2008) and Torrence and Compos (1998), Booth et al. (2009) attempt is interested in identifying an previously unknowns scales of interest. And in much of the same way, all of these works are comparing two sets of spectra to identify the scales of interest. Torrence and Compos (1998) use a theoretical background red noise spectrum, while Perron et al. (2008) utilize a the spectrum derived from a theoretical fractal surface. In Booth et al. (2009) the background spectrum is the spectrum of the pervious landscapes which are at a low risk of landslides. This work emphasizes for the purposes of this thesis the importance of selecting a background spectrum in order to make reasonable observations of the landscape. Without a

reasonable background spectrum, there would be no measure in place to be able to accurately identify important scales, other than through amplitude of the power spectrum at different scales, which in most landscapes is bias towards large scale features.

In addition, Booth et al. (2009) use the full-width at half-maximum (FWHM) technique to determine the range of scales that are relevant. Once a scale is compared to a background spectrum, clear areas of peaks tend to develop. While other tests such as the inverse-chi square test can be used to determine whether spectrum is most likely a true signal and not from randomness, it could still be difficult to differentiate the extent of the significant scales. To deterine the extent of significant scales, Booth et al. (2009) use the FWHM technique by identifying a peak maximum in the normalized power spectrum, then identifying the significant scales if they had a spectral power that is at least half of the maximum.

The study of Booth et al. (2009), while similar to the goal of this thesis, has a few significant differences. It does not attempt to identify characteristic scales; rather, it aims to use the wavelet analysis as a classification technique in determining landscapes. On the other hand, this thesis study aims to develop a tool improve the understanding of characteristic scales of landscapes. The thesis builds upon the framework of Booth et al. (2009) to develop an algorithm that identifies the characteristic scales in DEMs.

CHAPTER II

METHODS

2.1 Datasets

The input data for the required as inputs for the Fourier and wavelet analysis comprise of two-dimensional arrays, either representing real or synthetic topographic surfaces also known as a Digital Elevation Models or DEM. Synthetic DEMs with known characteristic scales have been created to verify the accuracy and capability of the algorithms. Next, DEMs representing synthetic river floodplains that are created using the Howard Model (Howard 1996) are used to identify the characteristic scale as well as better understand which surface properties or characteristics that are associated with the characteristic scale.

2.1.1 Synthetic Test Surfaces

The algorithm is tested and verified against a 1024 by 1024 image of two perpendicular sin waves, one with a wavelength of approximately 128-pixels and the other with a wavelength of 32-pixels, with the longer wavelength having an amplitude twice as large as the smaller wavelength (Figure 2 and Figure 3). A test image with identical characteristics was also used in Perron et al. (2008) to verify the efficacy of their algorithm. In turn, this paper will use the known parameters of the test time to verify the algorithms used in this paper, in addition to comparing the results to Perron et al. (2008).

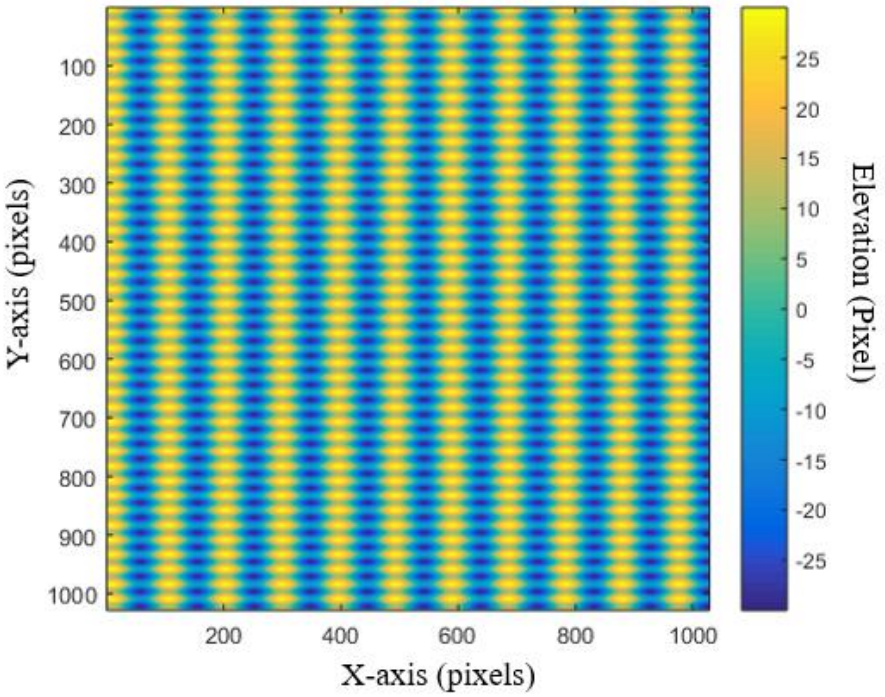

Figure 2. 2D representation of sine-wave test image

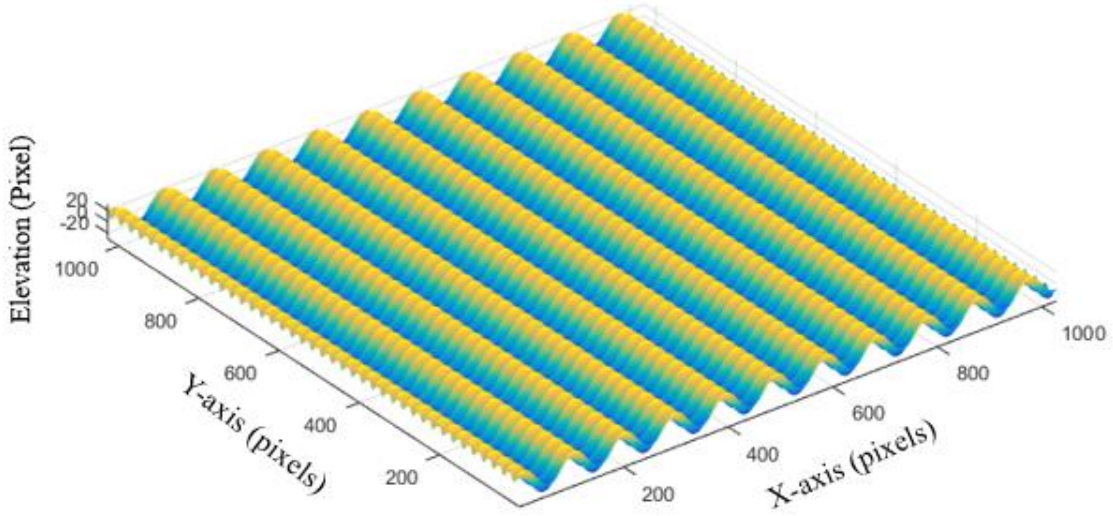

Figure 3. 2.5D representation of sine-wave image test image

To further understand the capabilities of this algorithm, varying amounts of white noise have been applied to the original dataset, with a total of 5 variants. The first has no noise applied to it, the second has a signal to noise ratio of 10:1, the third a, S/N ratio of 1:1, the forth 1:10, and the fifth 1:100 (Figure 4 and Figure 5). The varying levels of noise will help identify approximately an approximate S/R ratio that this algorithm is able to still detect the characteristic scale of the actual signal versus randomness or noise in a landscape.

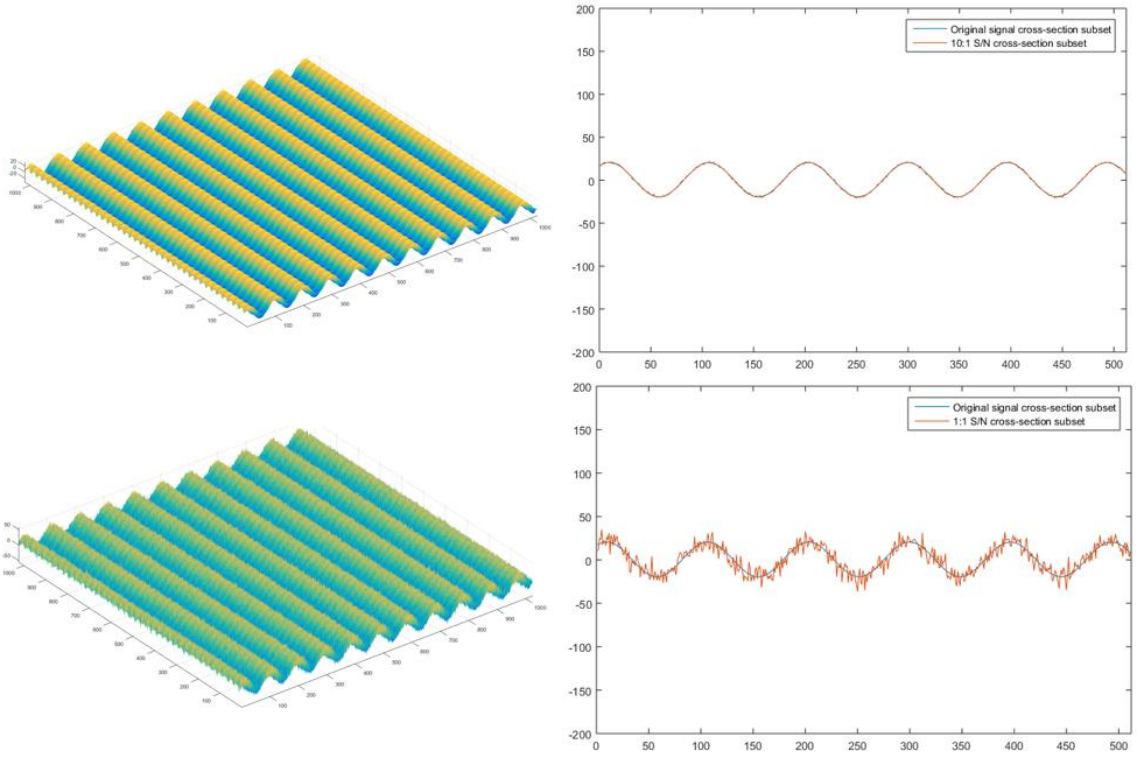

Figure 4. Sine-wave test image and 1D transect with 10:1 and 1:1 S/N ratio

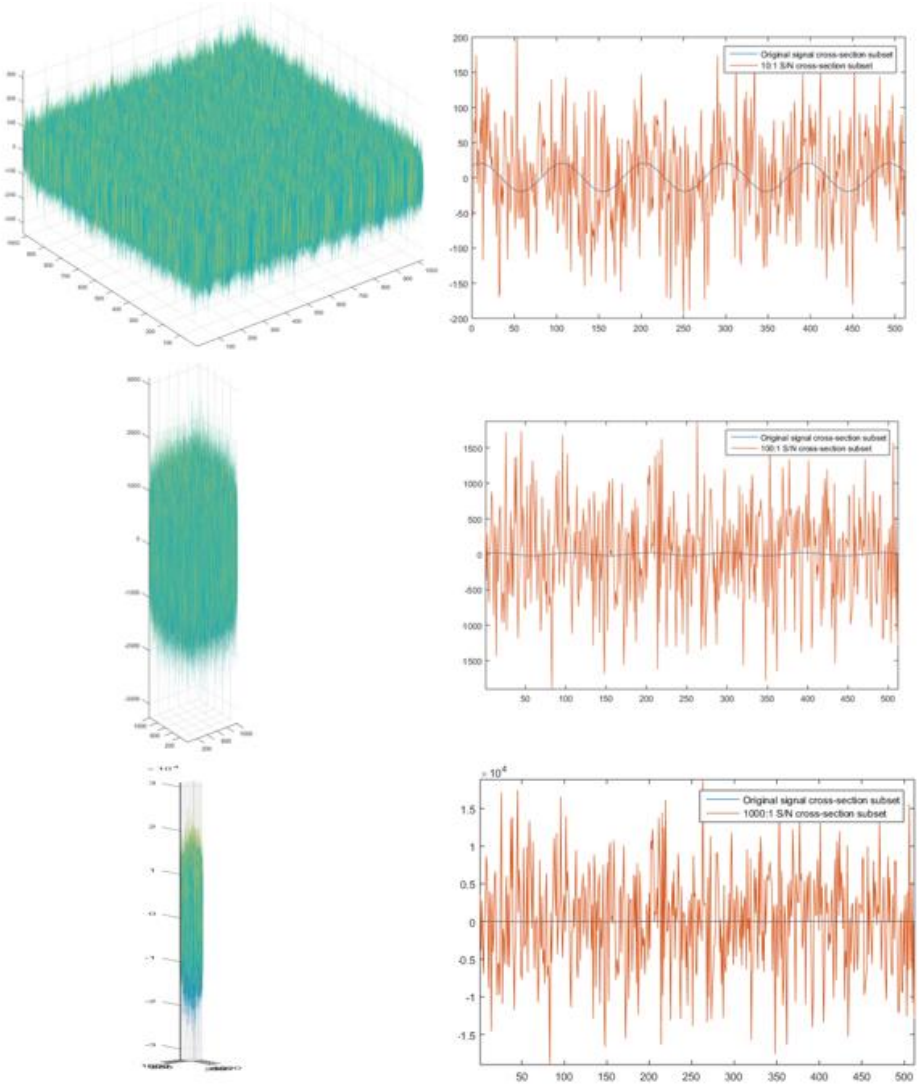

Figure 5. Sine-wave test image and 1D transect with 1:10 and 1:100 S/N ratio

2.1.2 Fractal Surface with and without characteristic scale

To better mimic conditions that would be seen in a realistic environment, two 512 by 512 surfaces were generated that were made to resemble a landscape. The diamond square algorithm was used to create a purely fractal surface that portrays realistic landscape. A second surface was generated to have the same properties as the

first, with the exception with 5-10 pixel features randomly located across the image. The first fractal surface would not have a significant characteristic scale based on the definition given in this thesis. The second landscape, however, should have a characteristic scale of approximately 5-10 pixels (Figure 6 to Figure 8).

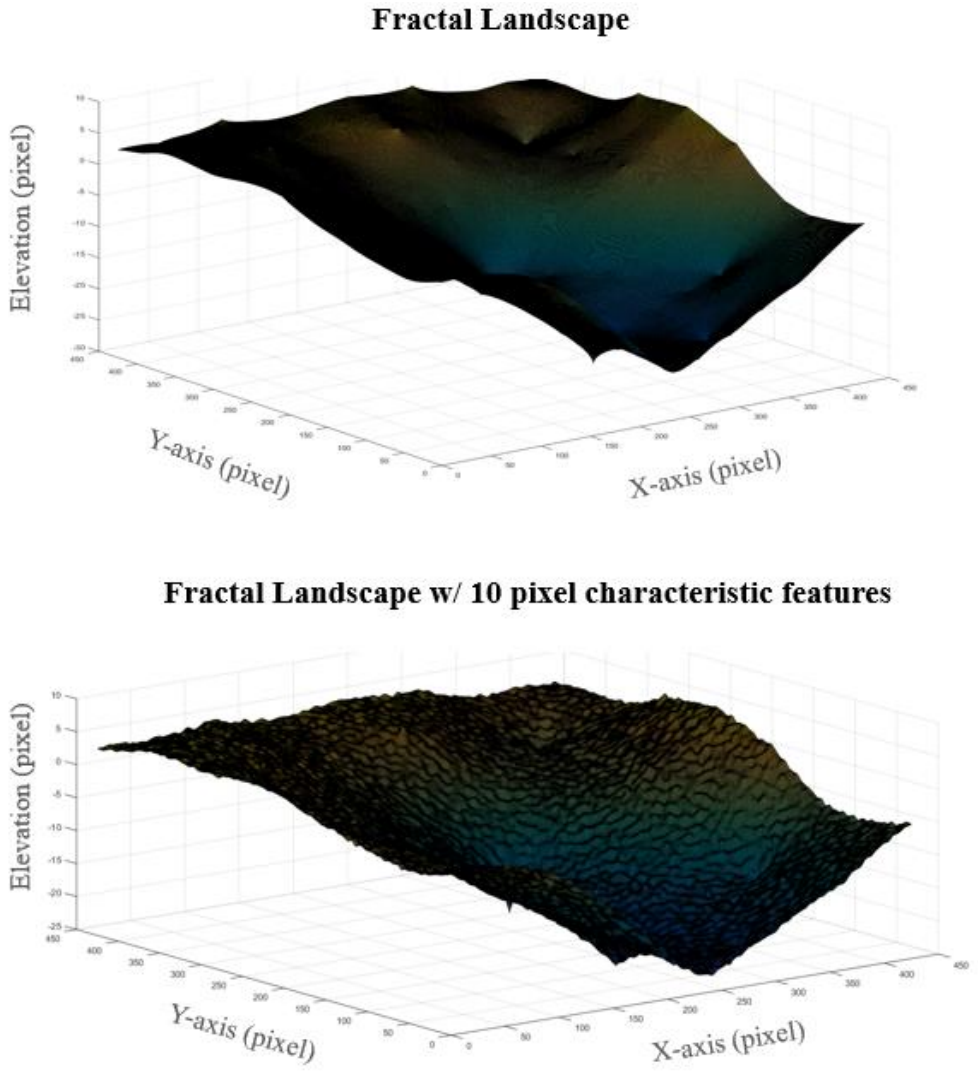

Figure 6. 2.5D representation of fractal test surface and fractal test with 10 pixels characteristic features with vertical exaggeration

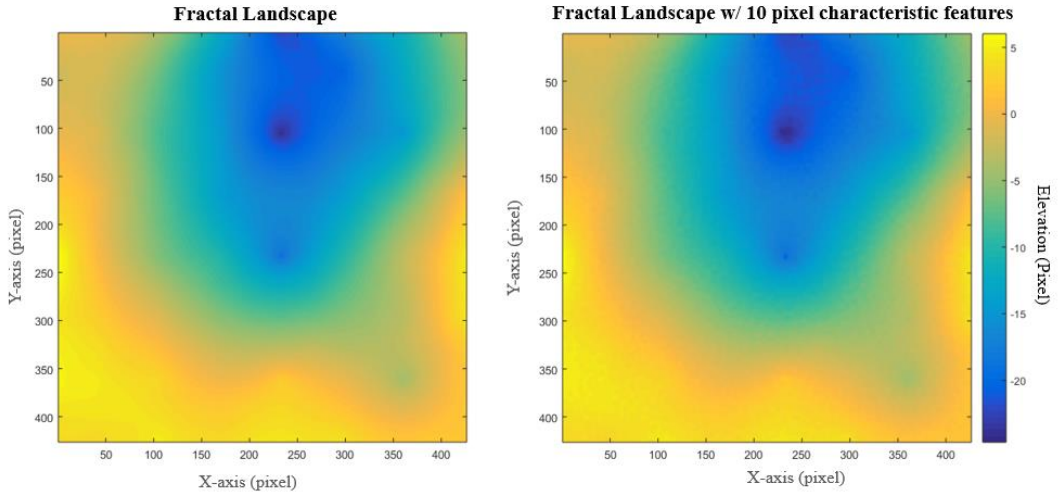

Figure 7. 2D representation of fractal image and fractal image with 10 unit characteristic scale

2.1.3 Synthetic River

The goal of this thesis is to utilize spectral analysis techniques in determining the characteristic scale of meandering river floodplains. Lidar DEMs of floodplains can be quite problematic for this purpose because most rivers have some anthropogenic influences or have a large number of vegetation around the banks which makes it difficult to understand the meandering river floodplain's three-dimensional structure. To isolate the key components of interest, in this study a synthetic river floodplain DEM was used. The synthetic floodplain was derived by using the floodplain evolution model developed by Howard (1996). The model is able to simulate the evolution of the planform and the floodplain topography of a meandering river. The model simulated the river which initialized as a straight planform with small magnitude random spatial perturbation. Over time, the river migrates and increases sinuosity to the point that neck

cutoffs start occurring. At the same time, it evolves the floodplain topography as the river migrates (Howard, 1996).

The model of Howard (1996) was used to perform the simulations over a total of 5000 iterations. The warming up period corresponds to the first 1000 iterations, in other words, after 1000 iterations, the model start generating river floodplain DEMs which exhibit developed meandering river planform including cutoffs. The model reaches to a stable state around 5000 iterations. Thus, the simulation was stopped at the 5000th iteration. The DEMs of the floodplain were generated every 250 iterations starting from the 1000th iteration to the 5000th iteration, focusing specifically on the final 5000th iteration. By conducting spectral analysis across these datasets overtime, patterns in the results will become more apparent and help better identify not only the characteristic scale but help identify the associated features. These can be seen in Figures 9 to 14.

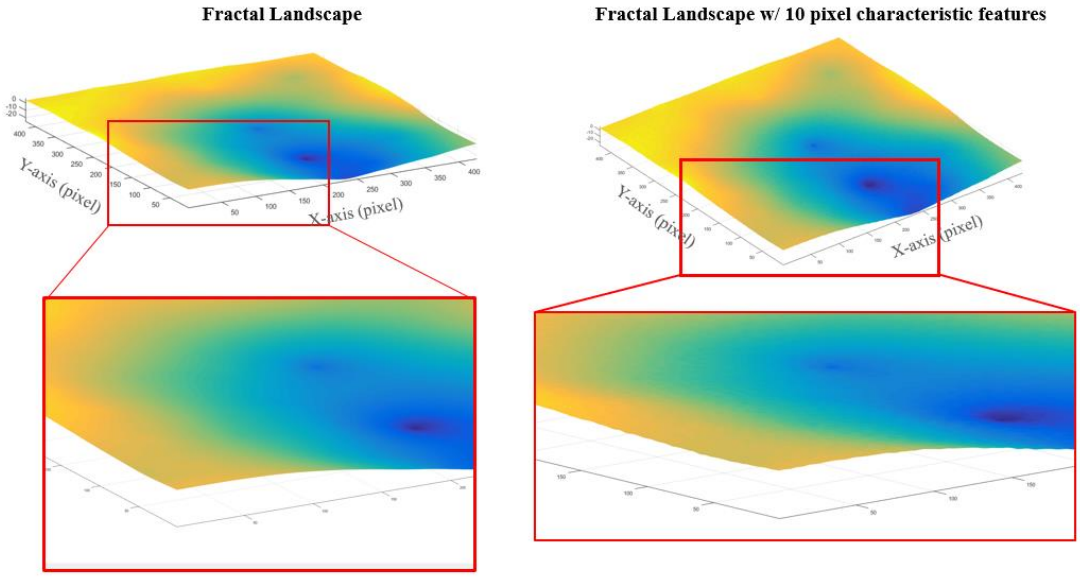

Figure 8. 2.5D representation of fractal test surface and fractal test with 10 unit characteristic features without vertical exaggeration

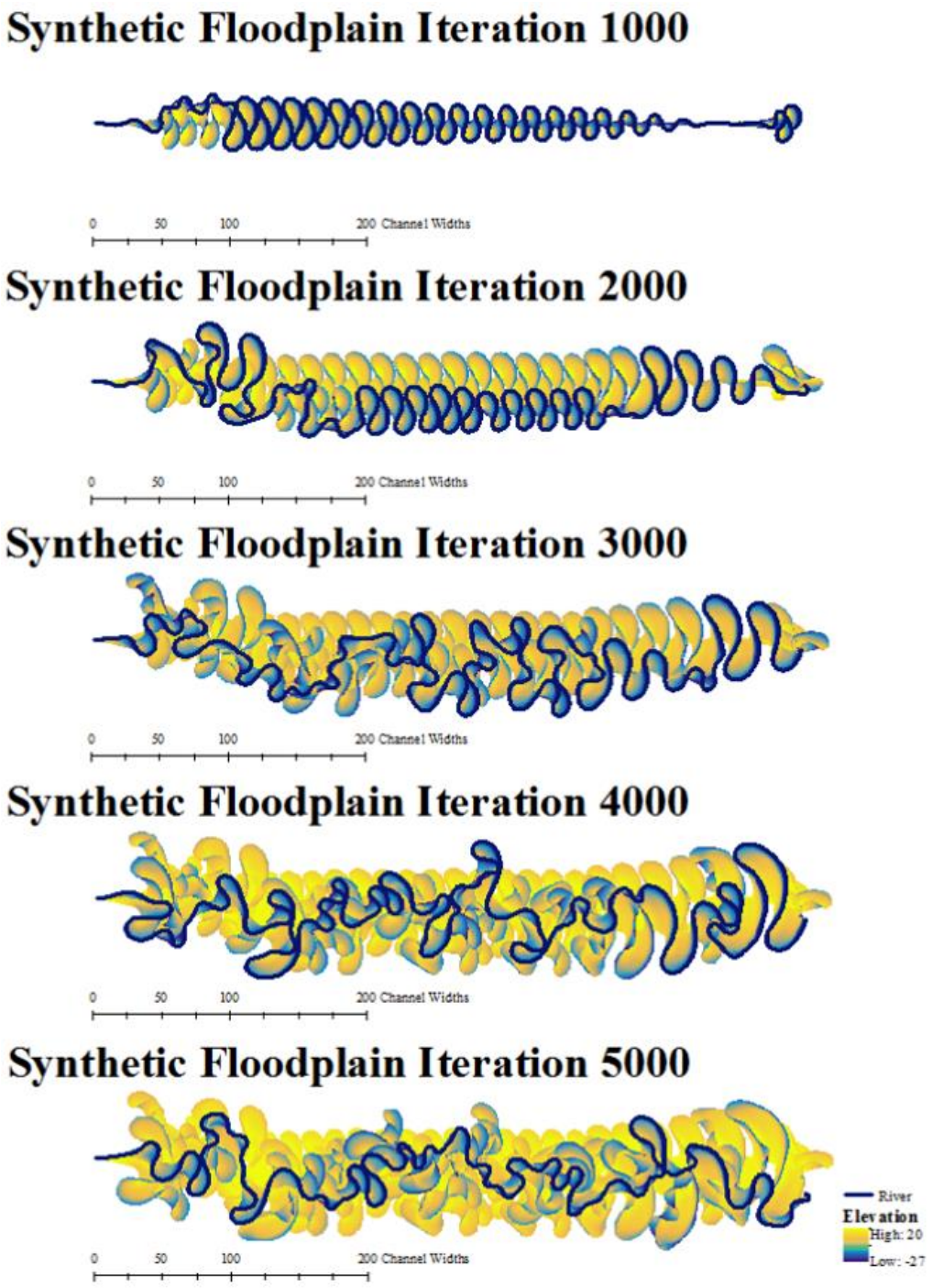

Figure 9. Synthetic river floodplain DEMs for every 1000th iteration from 1000 to 5000 iterations

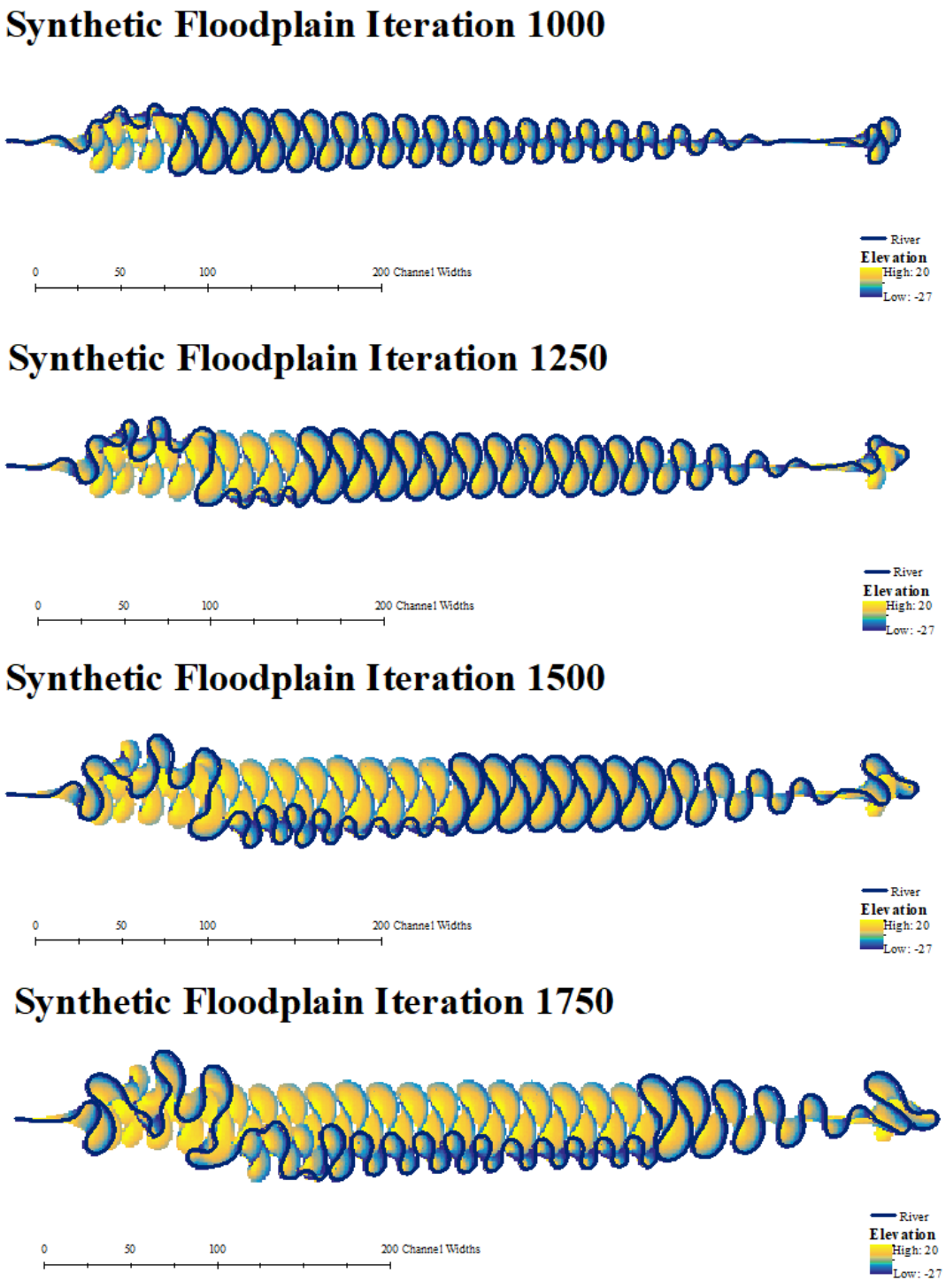

Figure 10. Synthetic river floodplain DEMs for every 250th iteration from 1000 to 1750 iterations

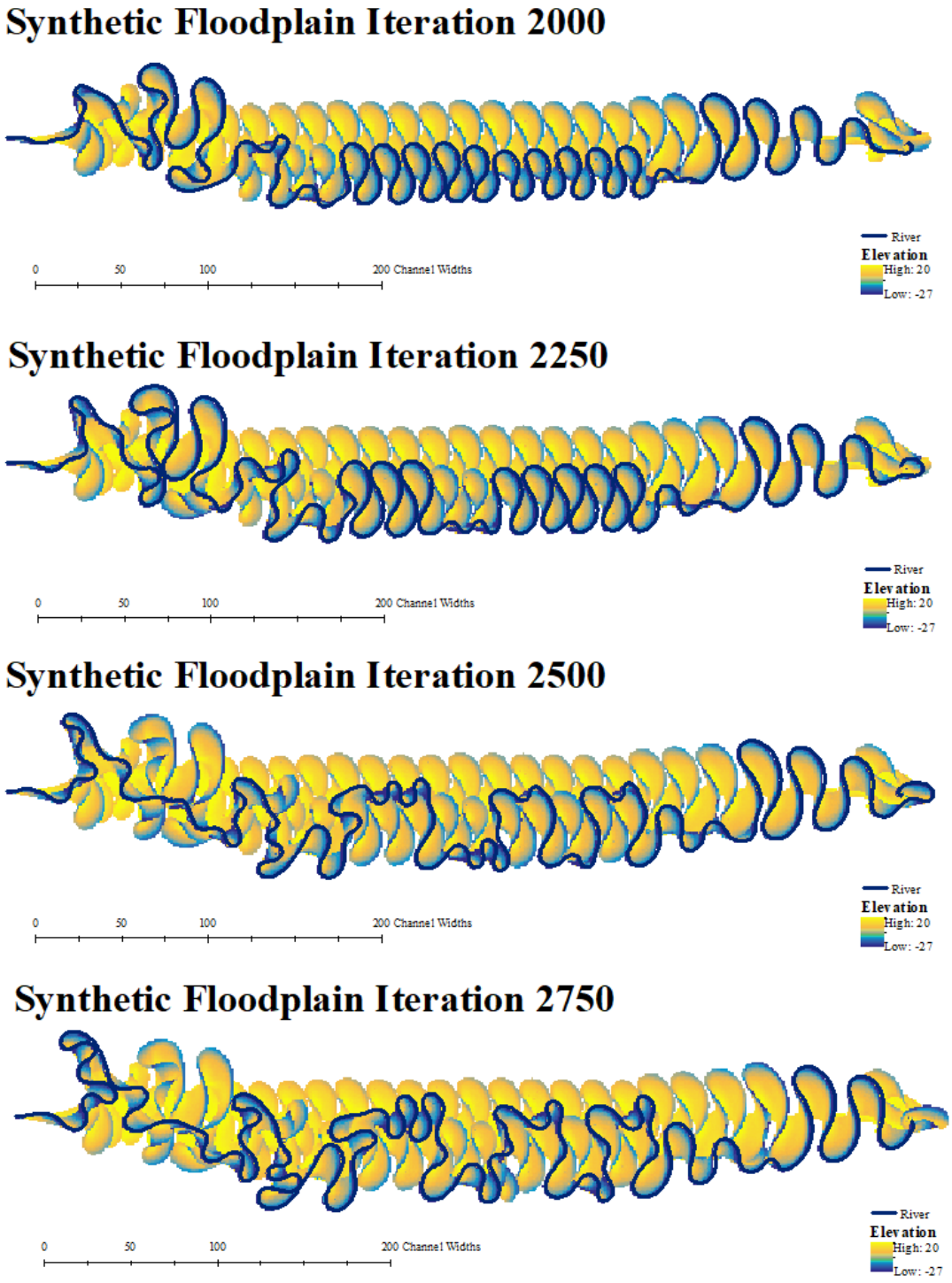

Figure 11. Synthetic river floodplain DEMs for every 250th iteration from 2000 to 2750 iterations

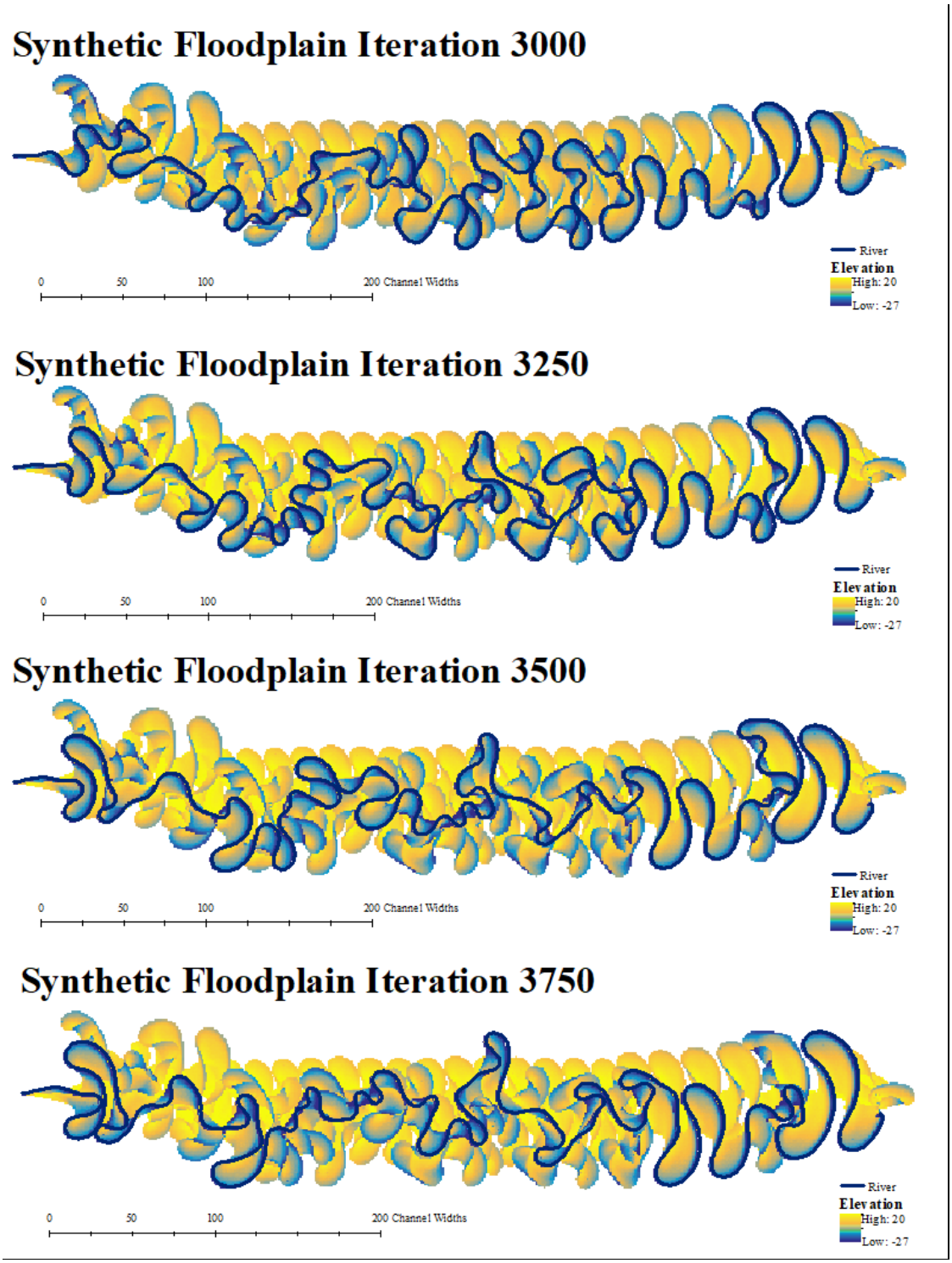

Figure 12. Synthetic river floodplain DEMs for every 250th iteration from 3000 to 3750 iterations

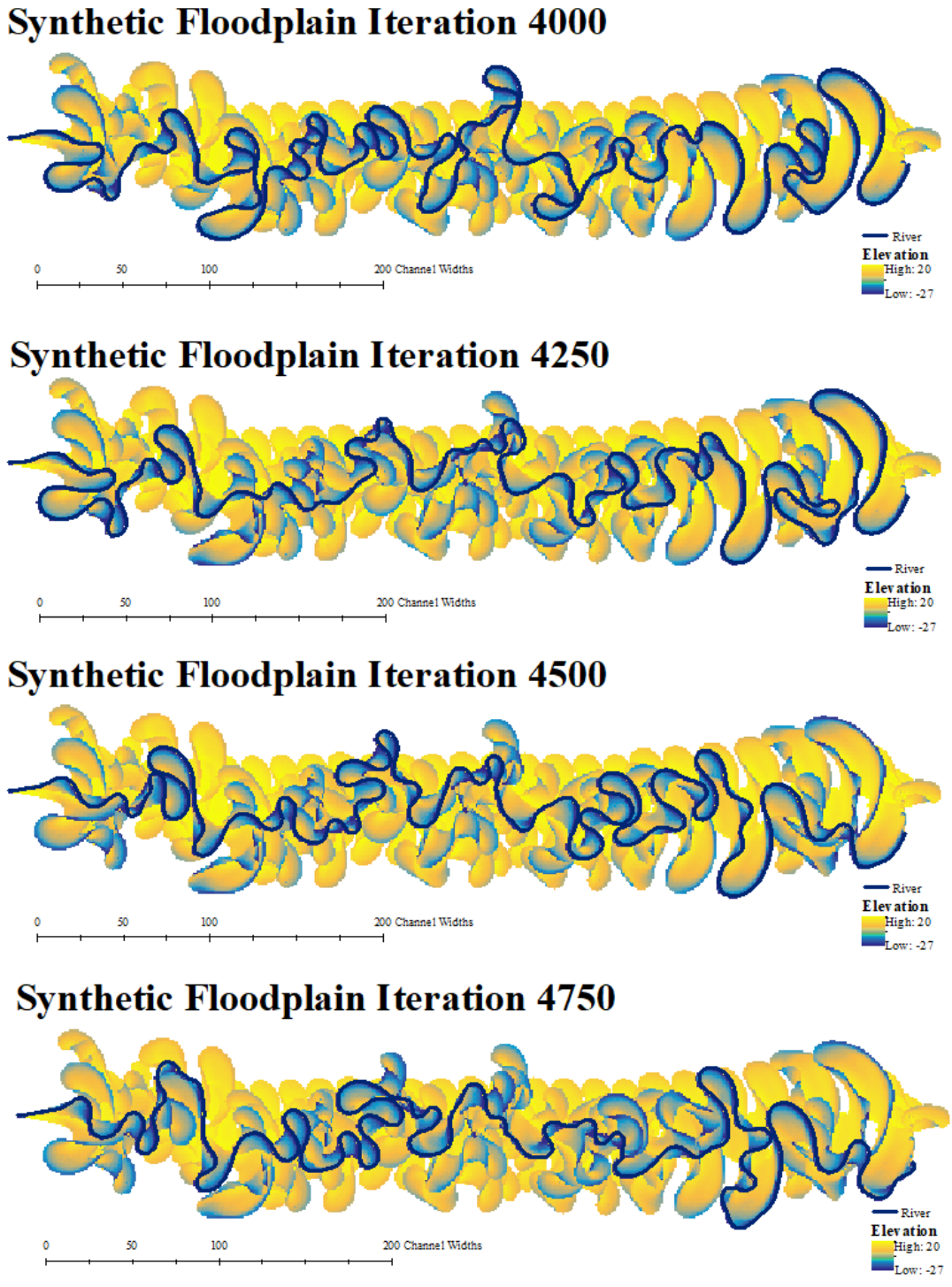

Figure 13. Synthetic river floodplain DEMs for every 250th iteration from 4000 to 4750 iterations

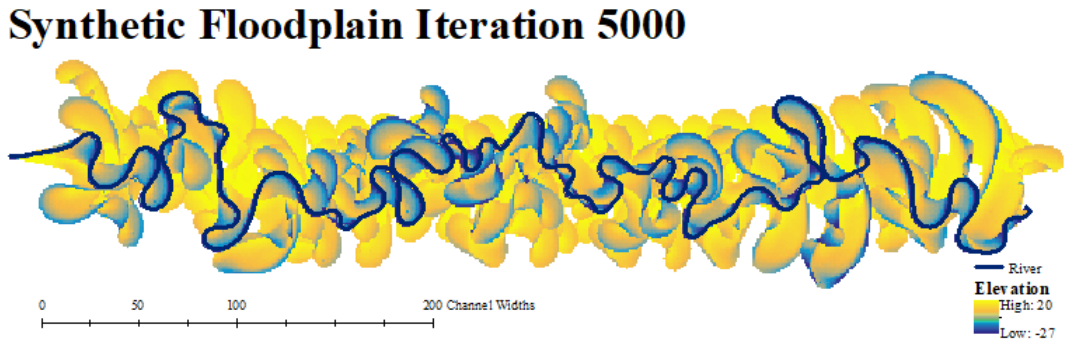

Figure 14. Synthetic river floodplain DEMs for the final 5000th iteration

2.2 Preprocessing Data for Spectral Analysis

As the datasets used for this project most of the datasets as synthetic, preprocessing is not mandatory with this data. However, preprocessing steps are applied to the data to keep the methodology consistent to how this algorithm would be used on a Lidar DEM, all dataset are preprocessed before use. The first step will be to detrend the data. The data will be detrended to avoid bias in the spectral analysis (Priestley 1981, Percival and Walden 1993). Next, pixel values should be normalized between 0 and 1. This is done to keep the range of values in a similar range to that which is being used for the background spectrum.

If a real-world DEM were to be used, it should first be studied to identify errors and anomalies in the dataset. Erroneous pixels or measurements must be removed and have their values interpolated.

2.3 Identifying characteristic scale with Fourier analysis algorithm

After the data is preprocessed, Hann cosine window is applied to the data to pad the dataset to help reduce any edge effects associated that could result from the Fourier

transform. The discrete Fourier transform is performed on the preprocessed data. The Fourier coefficients are then converted into the two-dimensional power spectrum (Equation I-12). The spectrum results to view 1D plot of the radial frequency, can is useful to view which scales are dominant, irrespective of orientation.

As mentioned previously, it is difficult to interpret these results without establish a theoretical background spectrum. For this algorithm, the theoretical background spectrum is calculated numerically by generating 1000 red noise surfaces. The beta value for can either be set to a generic red noise surface (-2), pink noise surface (-1), or white noise (0), though for certain landscapes, a beta value which best fits the averaged binned mean values or by using Equation I-36 would be most appropriate in order to accurately identify characteristic scales. Once the surfaces have been generated, the Fourier transform (Equation I-3) is performed on each of the surfaces to generate the Fourier coefficients, which is then converted into the power spectrum (Equation I-12) is performed on the Fourier coefficients, which are then averaged to generate a theoretical background red noise spectrum. Now, the theoretical background spectrum can be used to normalize the power spectrum of the target landscape. Both a normalized 1D radial frequency results and the 2D power coefficients can be displayed. It is important to remember that the 2D power coefficient results are displayed in the frequency domain and do not give insights as to the location of what is driving those effects, though it does provide information as to the characteristic scales and their potential orientation. The 2D power coefficient results can also give insights as to the structure of the image, whether it is highly structured or if it is more random in its orientation or distribution.

An inverse chi-square (Equation I-39) can be used to establish confidence intervals which are used to determine if a certain power coefficient is indeed significantly above the background spectrum to be notable. In a random image, 1% of the power coefficients would be above the 99% confidence interval. Though if an image has an underlying process or exhibits a characteristic scale, a larger percentage of the power spectrum will meet or exceed the 99% confidence interval. After this, the full-width at half-maximum of power coefficients that are above the confidence intervals can be used to identify the range of scales that are characteristic. It is possible that a landscape has more than one characteristic scale. The scale with the highest spectral power is denoted as the global characteristic scale, while smaller scales are noted as local characteristic scale.

2.4 Identifying characteristic scale with wavelet analysis algorithm

After the data has been processed, the algorithm can begin. The continuous wavelet transform (Equation I-8) is applied to the data using the Mexican Hat wavelet (Equation I-9). The Mexican Hat wavelet was selected because of its prevalence in the geoscience literature (Wang and Lu 2009, Booth et al. 2009), it's high spatial accuracy (Torrence and Compo 1998), and the because the wavelet's shape mimics that of point bars and oxbows which are prevalent in the meandering river floodplain. Equation I-39 is then applied to the wavelet coefficients to obtain the power coefficients. As mentioned previously, the result of a 2D continuous wavelet transform is a 3D wavelet coefficients, with the X and Y relating to the X and Y location on the input image, and

the Z relating to the scale. The wavelength equivalent of each scale can then be calculated (Equation I-37) to easily compare the results to the Fourier analysis.

To do meaningful analysis of the wavelet power spectrum results, a background spectrum must be calculated first by generating 1000 wavelet noise surfaces. Just like for the Fourier transform, the beta value to set the degree of redness can either be set to a generic red noise surface (-2), pink noise surface (-1), or white noise (0), though for certain landscapes, a beta value which performed best for the Fourier analysis. The continuous wavelet transform (Equation I-8) is applied to the red noise images using the same wavelet (Equation I-9) used for the target landscape. The wavelet coefficients for each surface are converted into the power spectrum and then averaged with each other. Once the background spectrum has been established, it can be used to normalize the power spectrum of the input DEM. Because the result is a 3D data cube of power coefficients with each Z representing a different scale. The results can either be displayed in 1D, 2D, or 3D visualizations.

For a 1D representation, the power coefficients at each scale can be averaged together to produce a global power spectrum which can be used to compare the spectra in a similar way as the 1D radial frequency display for the Fourier power spectra. In addition, 2D power spectrum can be viewed for each individual scale, showing where there are increases in power in regards to its XY location for a specific scale. If there are a range of scales of interest, 2D power spectra for each scale can be summed to achieve a summed power spectrum for a range of scales. Finally, the 3D data cube can be viewed in similar to a volumetric cube. The Matlab script sliceomatic.m was for 3D

analysis and visualization. The 3D analysis can show how scales change over scales and also in regards to the XY location of certain scales. This form of analysis can provide a good way to broadly view the data, though some forms of analysis can still be difficult in a three-dimensional space.

CHAPTER III

RESULTS

3.1 General overview of results

Both the Fourier and wavelet based algorithm performed an anticipated, with slight differences in performance in different aspects. Generally, the 1D global power spectrum appears to be more sensitive for the Fourier transform, which is good if the desired outcome is extremely subtle, but also might be more susceptible to noise. The wavelet 1D global power spectrum seems to give a more general idea of the global power and is less susceptible to noise, but also may make it difficult to detect certain real trends in the data. As for spatial representation, the 2D Fourier transform is not able to represent the power spectrum in a way that can preserve spatial information. While there are work-arounds available such as the sliding window Fourier transform, it would not be as effective for understanding the characteristic scale for the entire area and not an ideal solution for this application. The 2D continuous wavelet transform used as mentioned previously, produces a 3D cube of power coefficients, with the X and Y coordinates corresponding the image and the Z-axis corresponding to the scale. This cube can have individual "bands" in the data cube viewed two-dimensionally, or a 3D volumetric cube can be used. The following will show the results and the outputs for each of the datasets used in the thesis.

3.2 Sine wave test image

The sine-wave test image (Figure 2) is first used to determine if this algorithm is performing correctly. This same dataset has been used in Perron et al. (2008) so that the

Fourier results can be verified. The wavelet results should also reveal similar information. For the Fourier results, first is the 2D Fourier Power Spectrum before it is normalized (Figure 15). It is important to note that the results are in the frequency domain, which the closer to the center of the represent lower frequencies or longer wavelengths and the farther toward the edges represent higher frequencies or shorter wavelengths. Before it is normalized, it can already been seen that there are two major features in two different orientations, which represent the ~128-pixel feature and the ~32-pixel feature. Once it is normalized to the background spectrum (Figure 16), it can clearly be seen strongest components are the ~128-pixel features and the ~32-pixel feature.

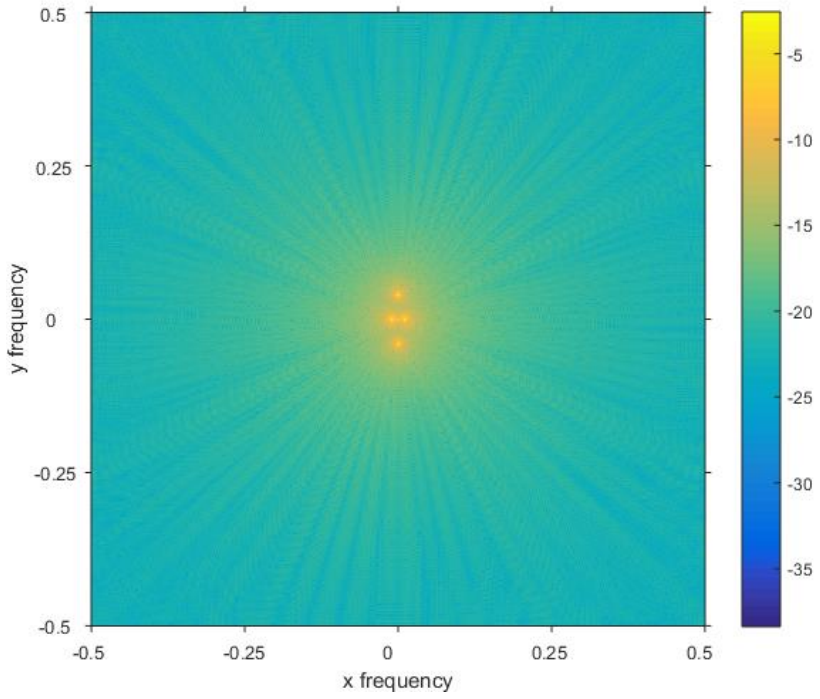

Figure 15. 2D Fourier power spectrum of sine-wave test image, before normalization. Yellow represents higher power and blue represents lower power

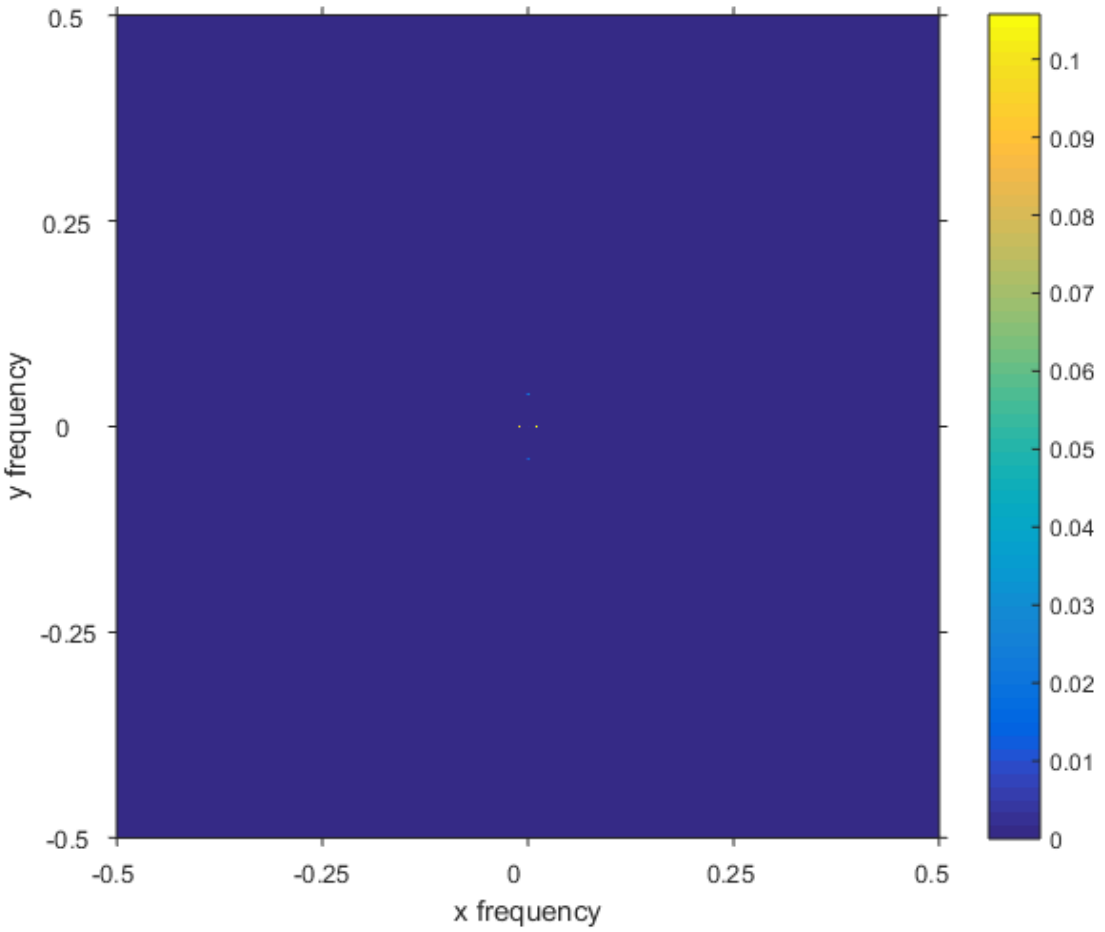

Figure 16. 2D Fourier power spectrum of sine-wave test image, after normalization. Yellow and blue circles represent significant components of the 2D power spectrum.

The power spectrum can also be represented in terms of radial frequency, which allows for a 1D presentation of the power spectrum. The power spectrum before it is normalized appears such as it does in Figure 17. Even in the unnormalized power spectrum, the two main peaks are associated with ~128- and ~32-pixel features. The black dotted line represents the background power spectrum. Once this is used to normalize the spectrum the result can be seen in Figure 18. Here, we have two main

peaks which are associated with both of these features. While the maximum Fourier coefficient is closer to ~100 pixel, the mean of the pixels is right at ~128-pixels. When examining the Fourier power spectrum, it is important to take both the maximum and the mean into consideration to have a full picture of what the 2D power spectrum is doing in the 1D power spectrum view.

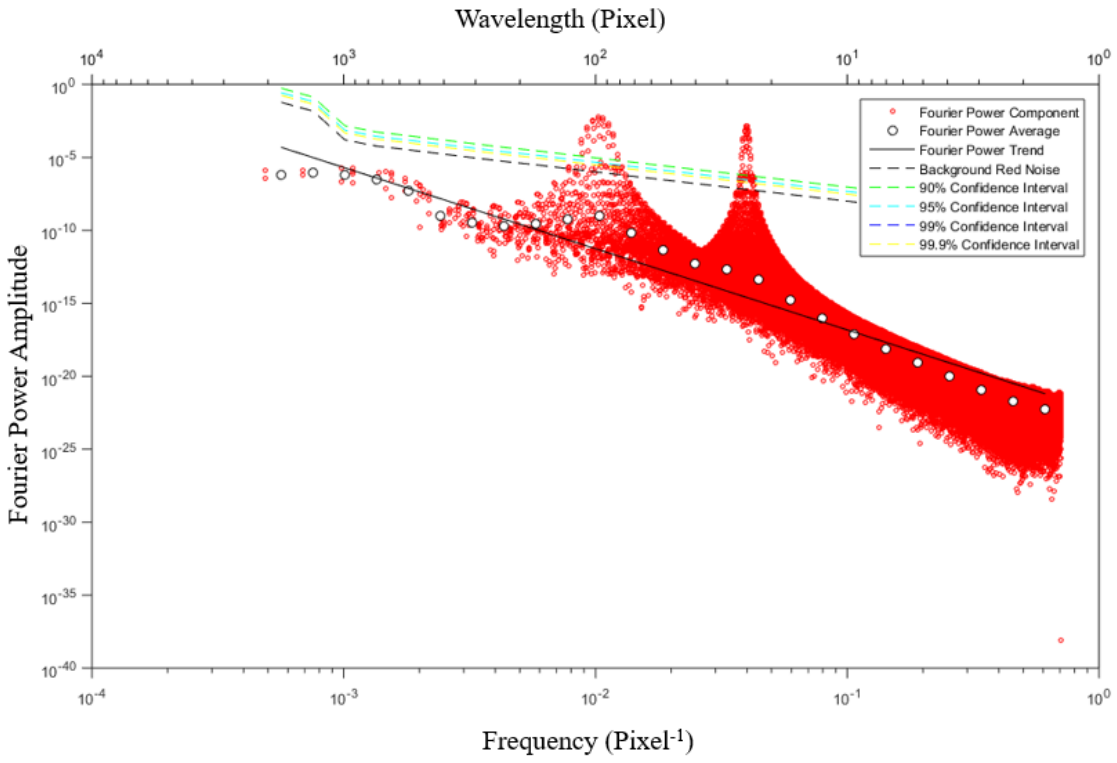

Figure 17. 1D Fourier power spectrum and background spectrum

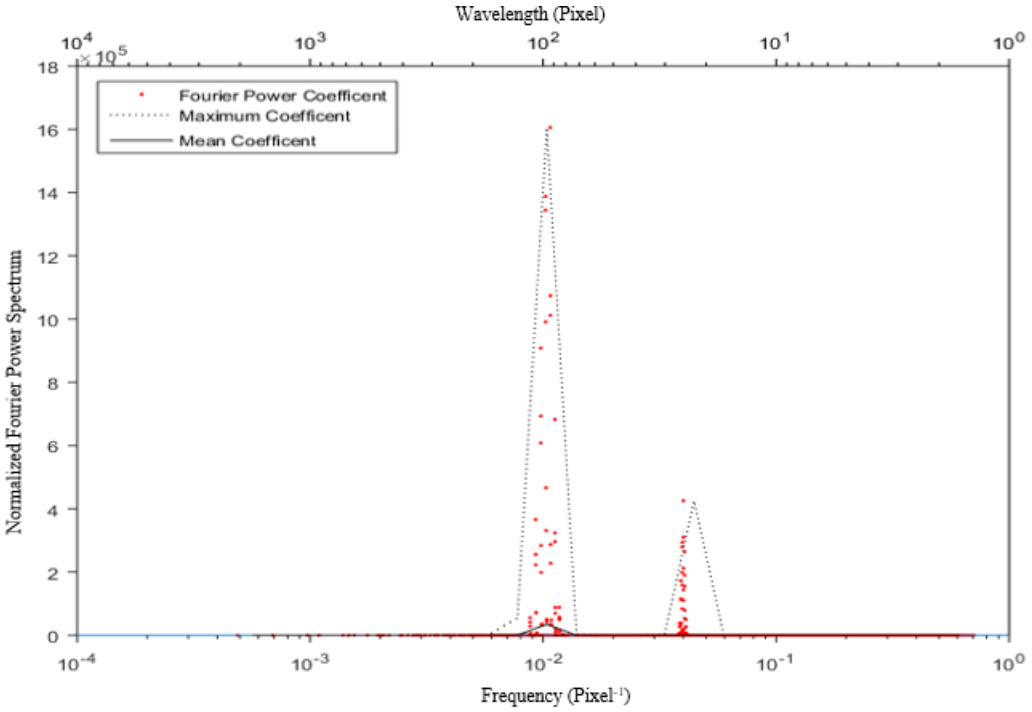

Figure 18. Normalized 1D power spectrum

A similar technique can be performed for the wavelet algorithm. As mentioned, the result of the 2D continuous wavelet analysis is a 3D cube of power coefficients. This cube can be viewed volumetrically, though it can sometimes be difficult to interpret the results. It is advisable to examine the 1D power spectrum first before examining the 3D power coefficient cube or examining individual 2D scales. The 1D wavelet power spectrum can be examined in a similar way as with the 1D Fourier power spectrum. The unnormalized 1D power spectrum can be seen in Figure 19, with the black line representing the 1D power spectrum and the red line represents the background red noise spectrum. Once normalized, the result can be seen in Figure 20. Here, we can see there is a very large peak representing the ~128-pixel feature and a smaller peak representing the ~32-pixel feature.

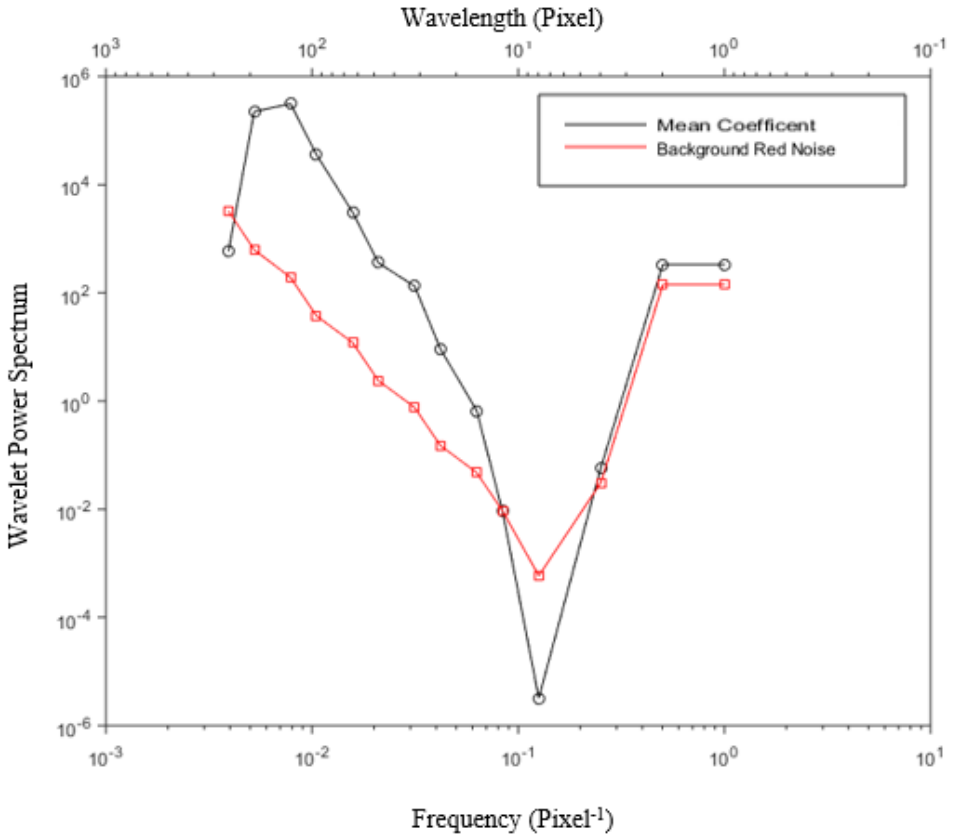

Figure 19. 1D wavelet power spectrum with the background spectrum

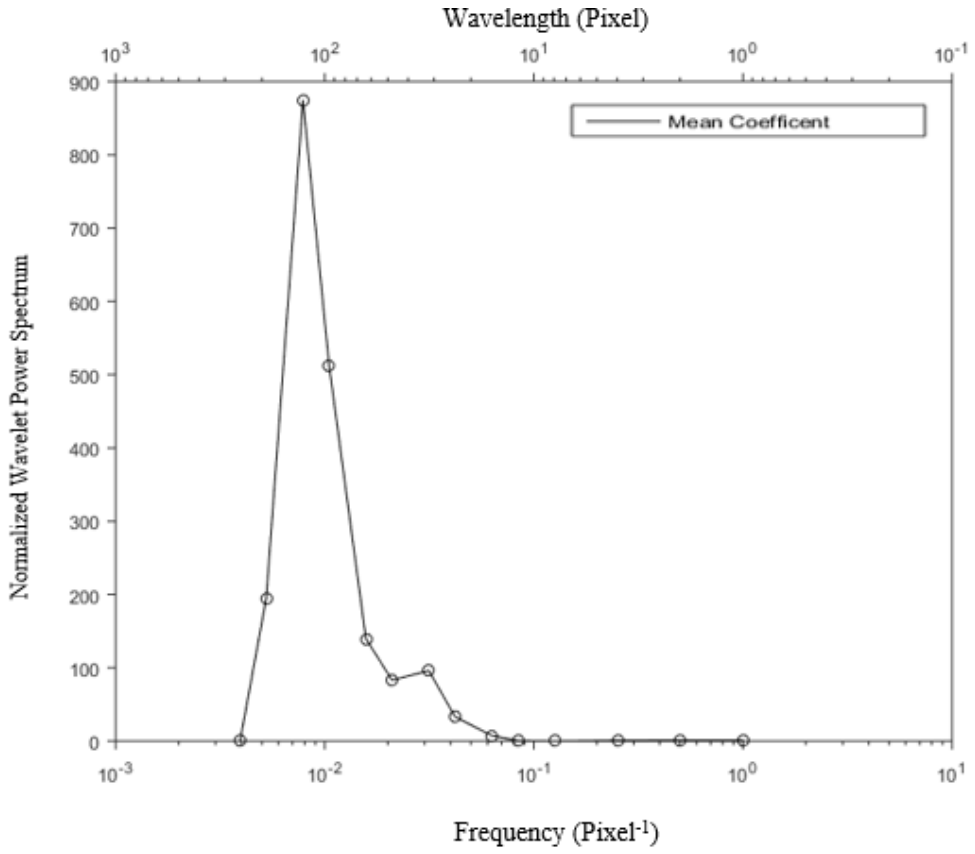

Figure 20. Normalized 1D wavelet power spectrum

The 2D power spectrum for each scale can also be viewed. In Figure 21 we can see the power spectrum for the 32-pixel scale and the 128-pixel scale. The 128-pixel scale the dominant scale, and its power spectrum clearly shows this. The 32-pixel feature is half the size and in a secondary feature in the landscape. The perpendicular 32-pixel feature is highlighted in the 32-pixel scale power spectrum, though it appears slightly distorted at regular intervals due to the influence of the dominate 128-pixel scale. The Mexican hat wavelet is ideal for detecting Gaussian features as opposed to sine-wave features. There may be another wavelet which would perform slightly better for this particular type of image, though as mentioned in a previous section, the Mexican

hat was specifically selected to handle the isotropic and Gaussian-like features that are prevalent in a meandering river floodplain.

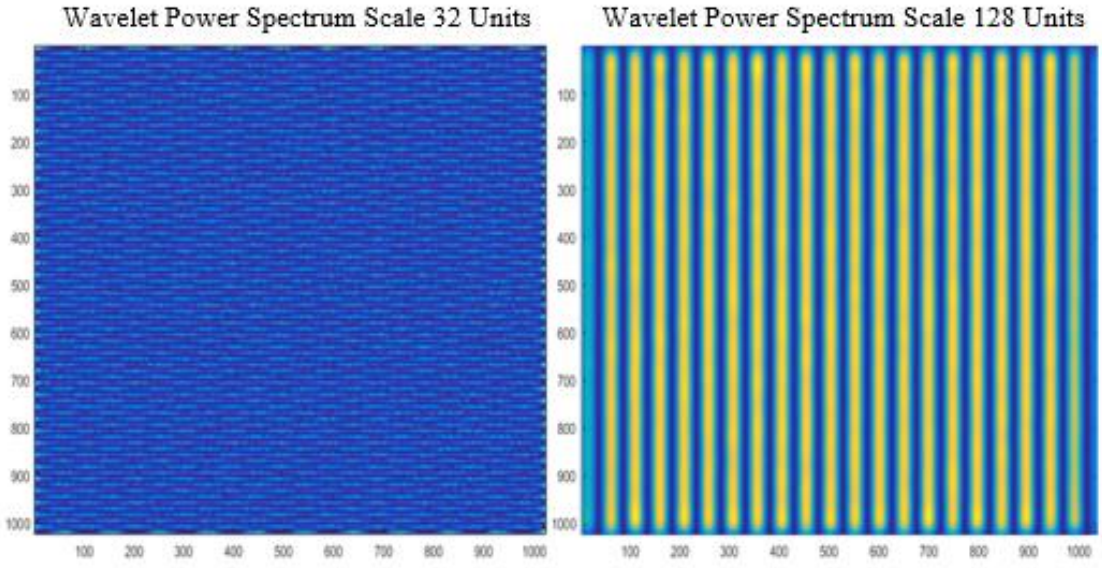

Figure 21. 2D wavelet power spectrum at scales 32 and 128 pixels.

While more difficult for quantitative analysis, the 3D power spectrum cube can be viewed as well. Figure 22 shows how the 3D power spectrum cube be viewed using a slice view, while Figure 23 shows it can be viewed using a volumetric view. In both causes, it provides additional information, though it works best in tandem in observing the 1D power spectrum and the 2D power spectrum at specific scales.

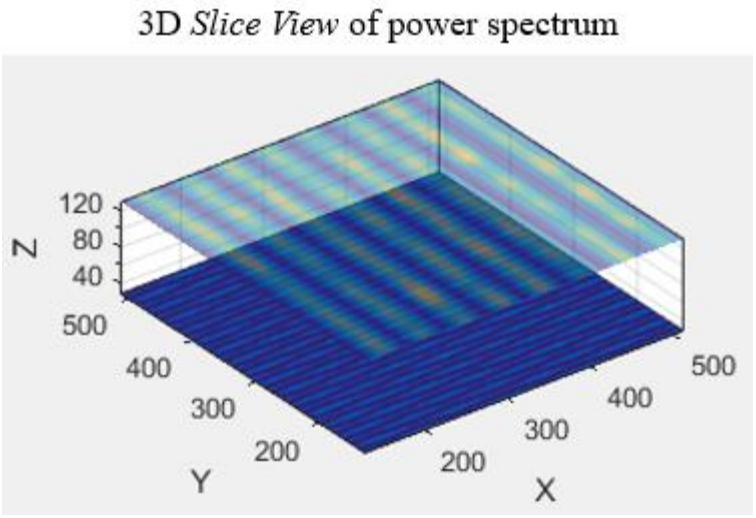

Figure 22. 3D view of wavelet power spectrum using a slice view

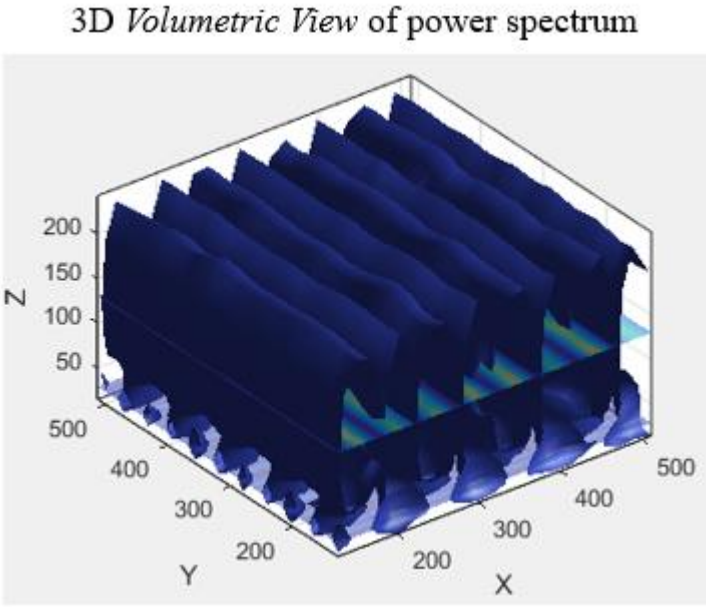

Figure 23. 3D view of wavelet power spectrum using a slice view

3.3 Sine wave test image with varying levels of noise applied

The same sine-wave image is then tested again with varying levels of white noise applied. The signal to noise ratios include 10:1, 1:1, 1:10, 1:100 and 1:1000. Figure 24 and Figure 25 show the 10:1 and 1:1 S/R ratio test images. Both of these appear almost identical without much difference between the two. Slight levels of noise can begin to be detected at 1:10 which can be seen in Figure 26, with the Fourier plot showing small amounts of noise. This can be seen in the Fourier results with a slightly dampened response at the ~32 unit scale. This dampening at the smaller characteristic scale is more evident with the wavelet power spectrum in which the ~32 unit characteristic scale is significantly dampened. At 1:100 Figure 27, the noise begins to inundate the signal itself, which can be seen in the Fourier results, though the scale is still detectable, as well as with the wavelet transform, though deciphering characteristic scale becomes more difficult. By the 1:1000 S/R ratio seen in Figure 28, the noise completely inundates the signal in the Fourier transform, though with the wavelet analysis it is still just barely visible. Detecting the characteristic features even with a 1:100 S/R ratio indicates that a characteristic scale can be identified in a particular image, even with high noise.

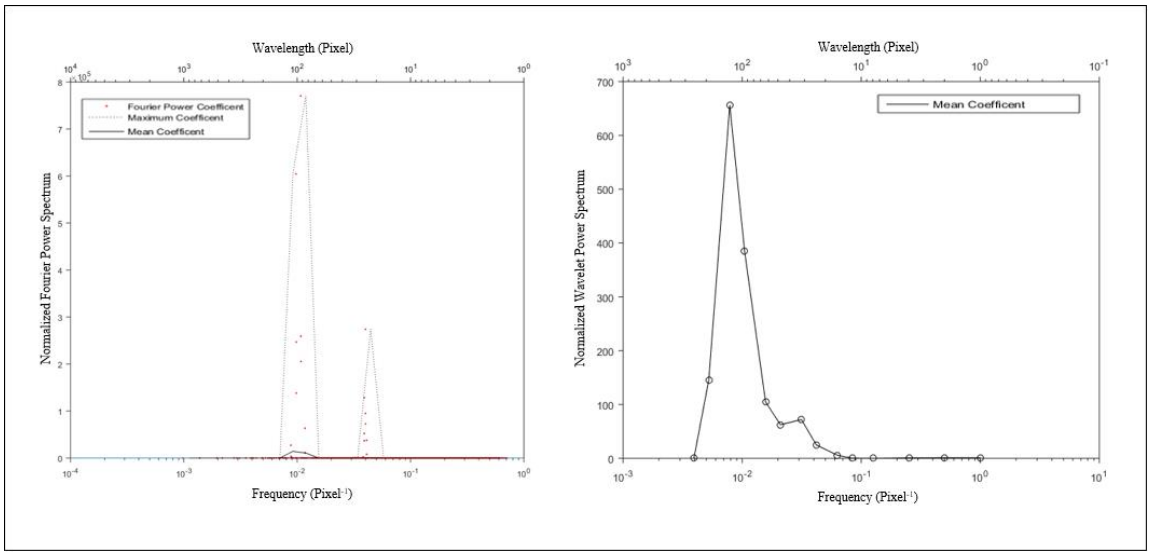

Figure 24. 1D Fourier (left) and wavelet (right) power spectrum for the 10:1 S/N ratio of the sine-wave test image

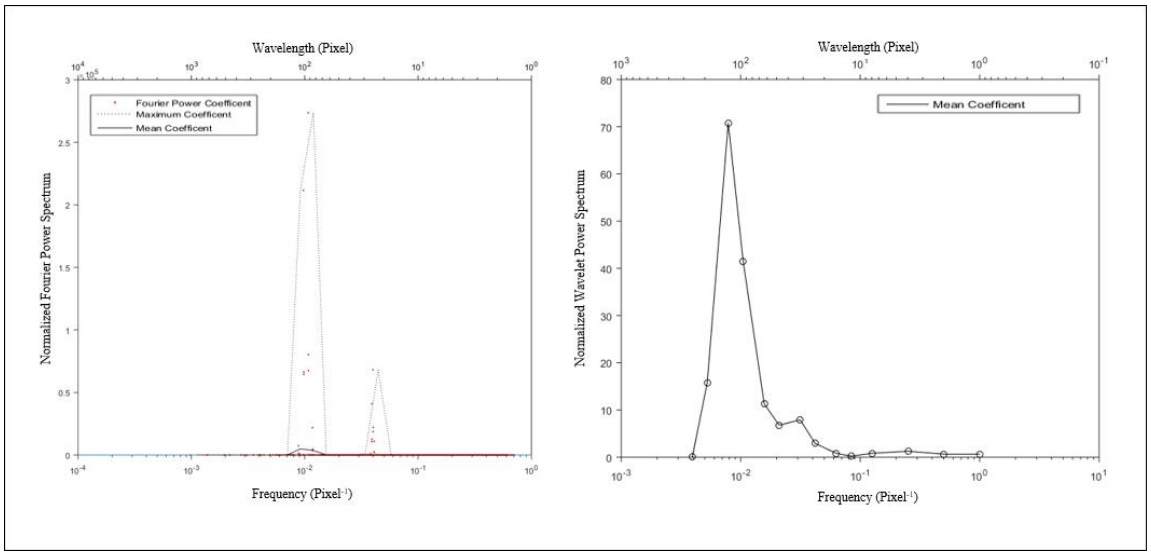

Figure 25. 1D Fourier (left) and wavelet (right) power spectrum for the 1:1 S/N ratio of the sine-wave test image

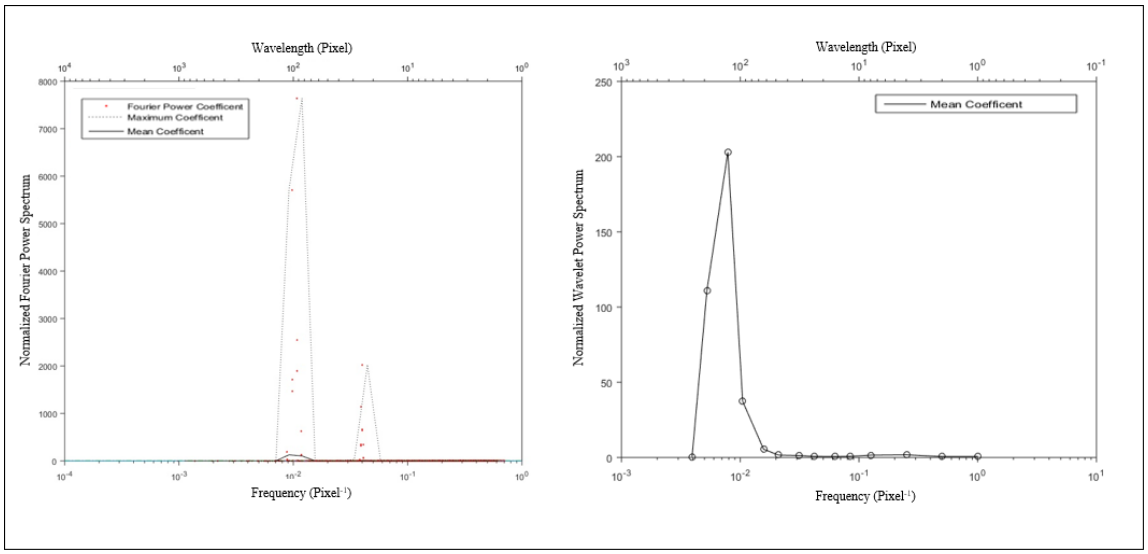

Figure 26. 1D Fourier (left) and wavelet (right) power spectrum for the 1:10 S/N ratio of the sine-wave test image

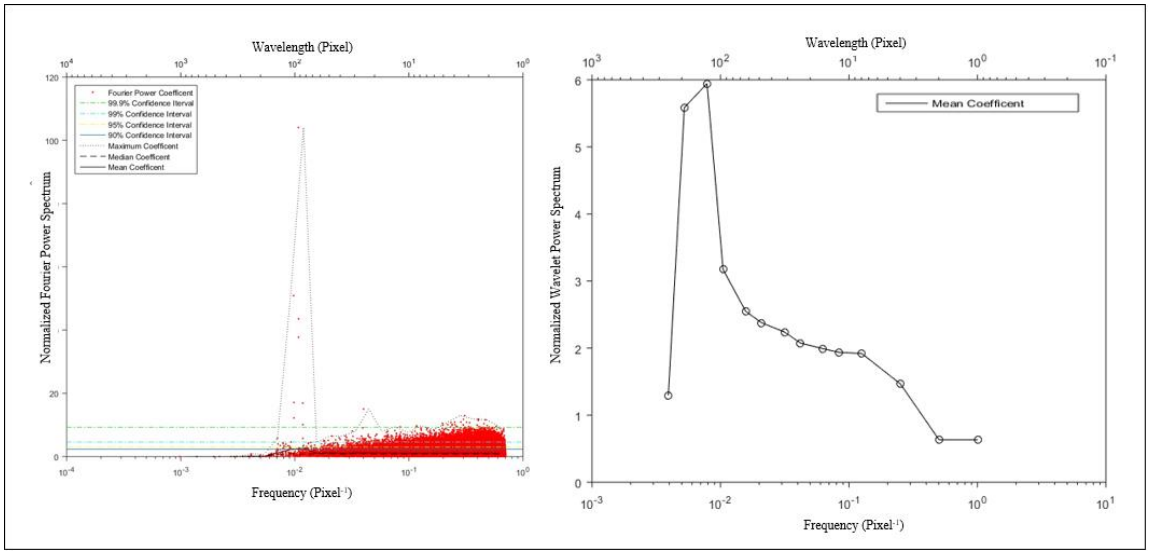

Figure 27. 1D Fourier (left) and wavelet (right) power spectrum for the 1:100 S/N ratio of the sine-wave test image

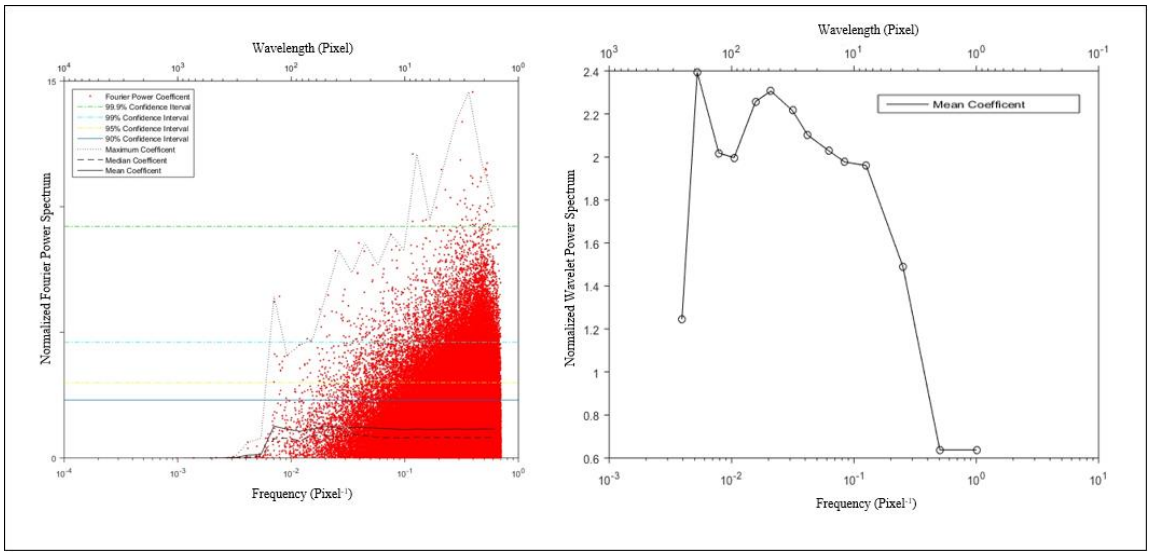

Figure 28. 1D Fourier (left) and wavelet (right) power spectrum for the 1:1000 S/N ratio of the sine-wave test image

3.4 Fractal surface with and without the characteristic scale

To examine how this would work on a more-realistic landscape, two surfaces were created to mimic a real world surface. The first is a fractal surface that is created using the diamond-square algorithm. The second image was the same image with 8-10 pixel Gaussian features randomly placed throughout the image. The 1D results show that it was able to detect the characteristic scale in the second image, while not detecting a characteristic scale in the control image, which is seen in Figure 29. Specifically, the spectral results for the fractal surface with a characteristic scale shows an increase in the power spectrum at around 8 pixel wavelength, while in the fractal surface without a characteristic scale, this increase in the power spectrum is absent.

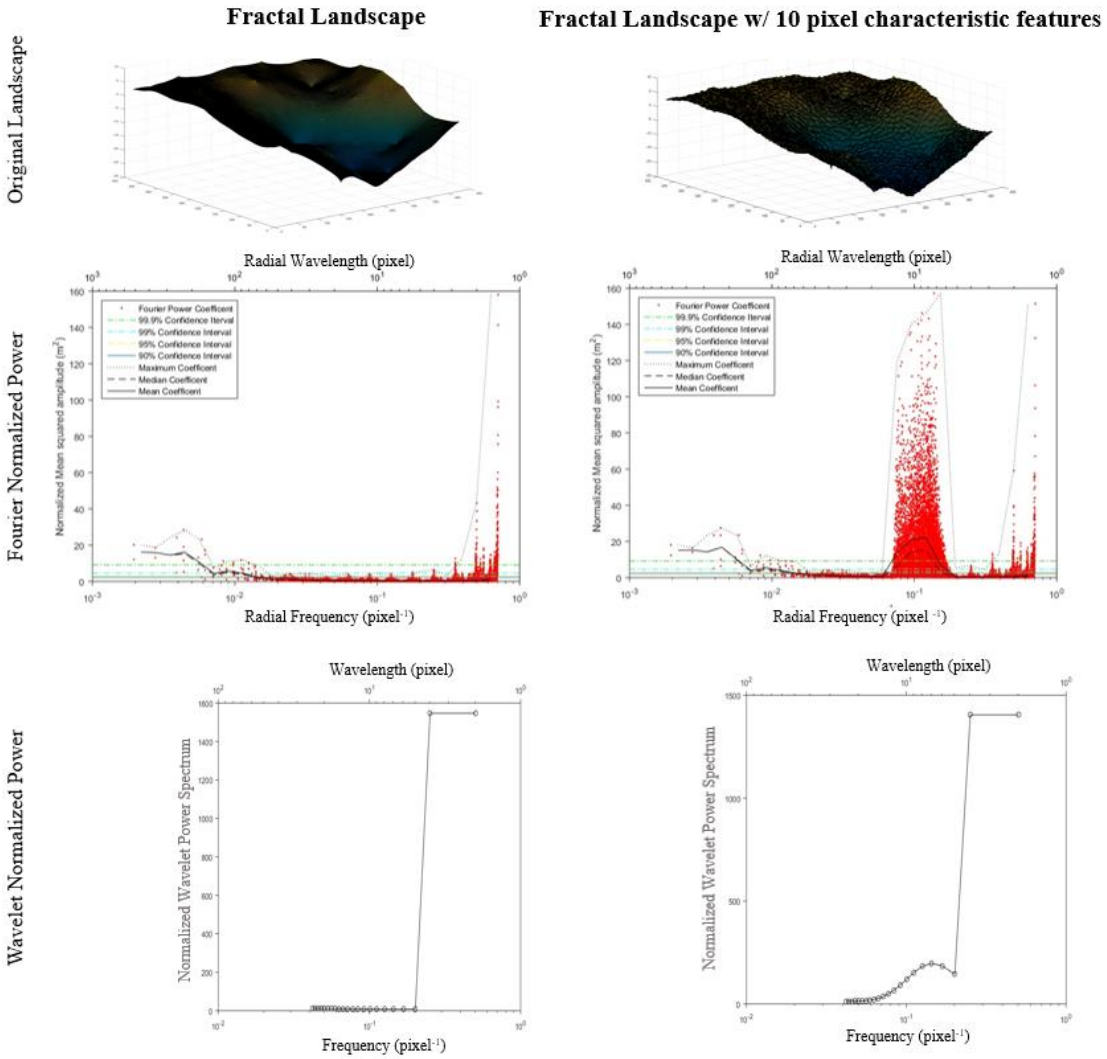

Figure 29. Fractal test images (top), the 1D Fourier power spectrum (middle) and the wavelet power spectrum (bottom)

3.5 Synthetic River Results

The Howard model outputs were processed using both the Fourier and wavelet algorithm. The results from the 1D normalized Fourier and wavelet power spectra of the DEMs generated at every 1000 iteration show that all spectra seem to have two peaks, one that typically around 8 channel widths to 16 channel widths, and a second peak that

we associate with larger wavelengths which is about 64 to 128 channel widths (Table 1, Figures 32-36). We describe the smaller wavelength characteristic scale as the bend-scale features and the longer wavelength features as the meander-train scale features. Using the FWHM of each peak of spectra, a corresponding range of characteristic scales for the smaller wavelength peak and the longer wavelength peak can be effectively established. While the inverse chi-square test can determine if a particular spike in spectra in significant, the FWHM can be used to more accurately define a specific range of scales that are most relevant. The characteristic scales for the meander-train scale and bend-scale features obtained from different iteration DEMs seems largely consistent although the higher the number of iterations to generate the DEM (i.e., the more mature the DEM), the wider apart these scales become (Table 1, Figures 32-36) Figure 30 and 31 show how the bend-scale and meander-train scales shift throughout the iterations.

Table 1. Lower and upper scales for each Full-Width at Half-Maximum (FWHM) for the bend-scale features and the meander-train scale features in addition to the peak power

	Bend-scale				Meander-train scale			
Iteration	Lower Scale	Upper Scale	Peak Power (10^6)	Peak Scale	Lower Scale	Upper Scale	Peak Power (10^6)	Peak Scale
1000	2.9639	15.8918	170.7733	3.9738	27.9264	136.1716	186.2003	63.58
1250	2.9639	17.9714	185.1660	3.9738	43.3289	123.9225	250.3503	95.37
1500	2.9619	21.8251	168.1546	3.9738	55.0694	186.0800	319.4820	95.37
1750	2.9642	17.9114	185.1660	3.9738	43.3289	167.2513	250.3503	95.37
2000	2.9627	23.6829	160.4132	3.9738	72.0500	222.2382	346.4457	127.16
2250	2.9636	24.3081	170.3976	3.9738	79.0886	233.6736	360.8980	127.16
2500	2.9628	29.7712	156.6655	3.9738	82.4254	161.0570	301.1117	127.16
2750	2.9363	24.3081	170.3976	3.9738	79.0886	233.6736	360.8980	127.16
3000	2.9634	36.6950	156.6482	3.9738	79.0886	233.6736	360.8980	127.16
3250	2.9634	34.2932	161.5491	3.9738	81.9762	271.2187	316.2396	127.16
3500	2.9635	30.9616	158.4586	3.9738	81.5176	280.8219	205.2612	127.16
3750	2.9634	34.2932	161.5491	3.9738	81.9762	271.2187	316.2396	127.16
4000	2.9638	43.6412	153.8334	3.9738	82.0264	300.7585	256.9377	190.74
4250	2.9630	38.9438	147.7062	3.9738	82.8444	301.1181	245.8300	190.74
4500	2.9977	31.6247	137.1392	7.9477	84.1215	299.2632	250.7427	190.74
4750	2.9630	38.9438	147.7062	3.9738	82.8444	301.1181	245.8300	190.74
5000	2.9611	25.6481	118.0192	3.9738	81.0393	297.9253	207.2034	190.74

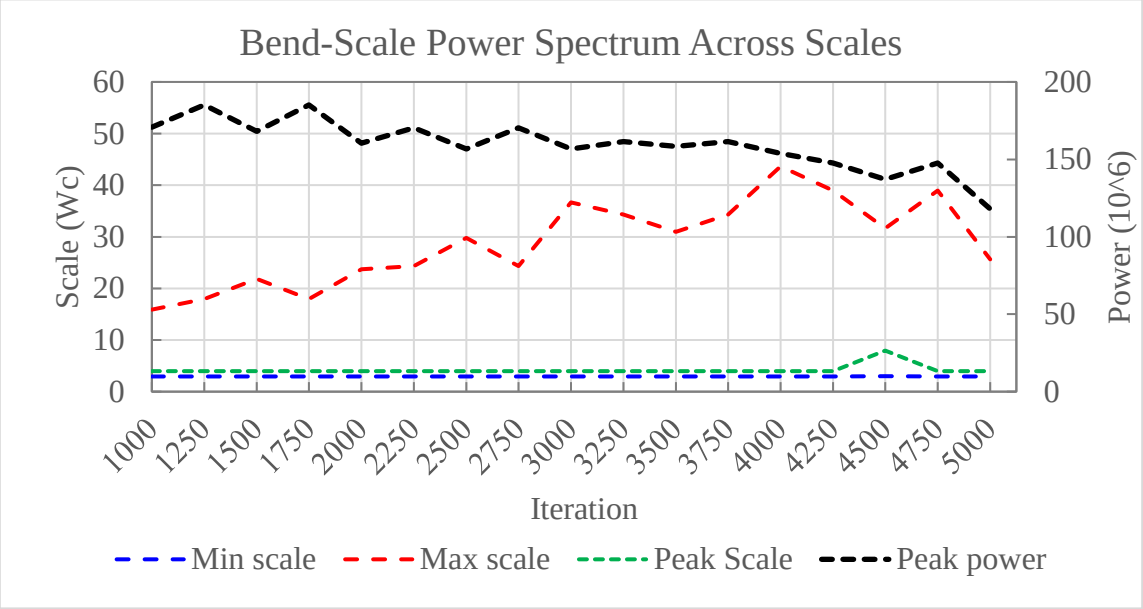

Figure 30. Chart showing the channel power spectrum across iterations, showing the scale at which has the peak power for the bend-scale features, the minimum scale, and the maximum scale.

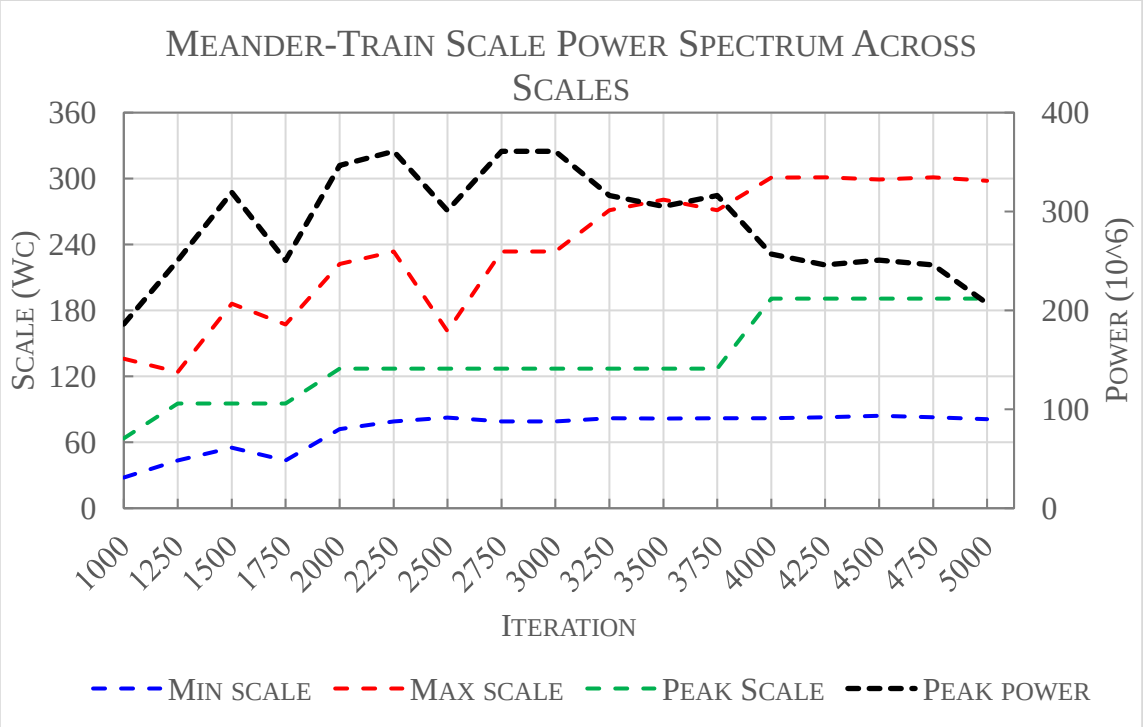

Figure 31. Chart showing the meander power spectrum across iterations, showing the scale at which has the peak power for the meander-train scale features, the minimum scale, and the maximum scale.

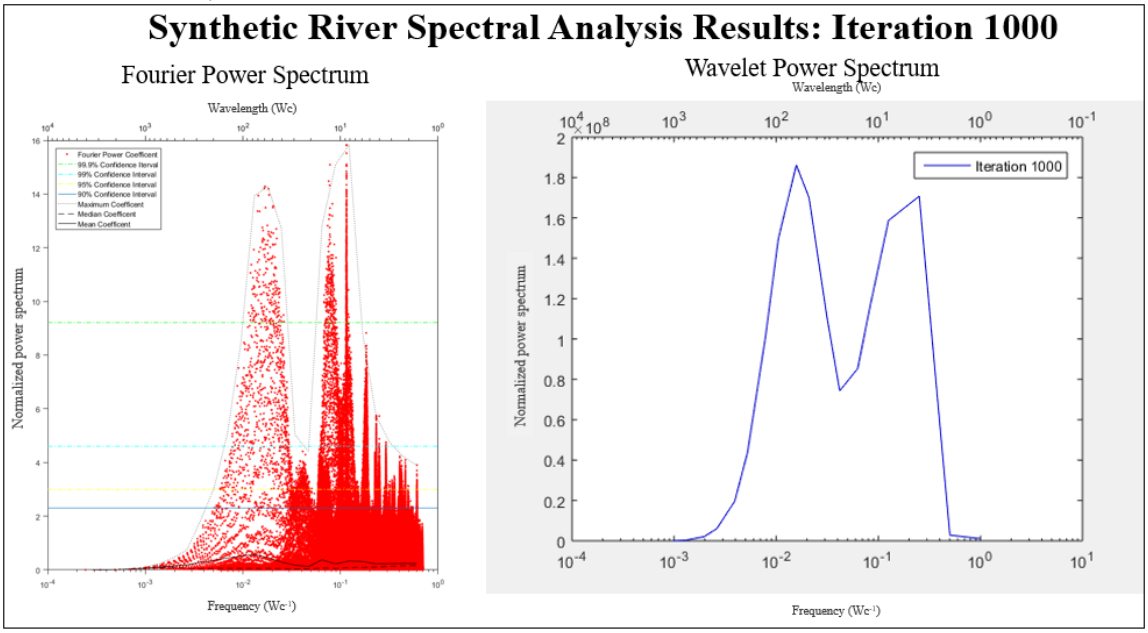

Figure 32. 1D Fourier (left) and wavelet (right) power spectrum for the 1000th synthetic river output

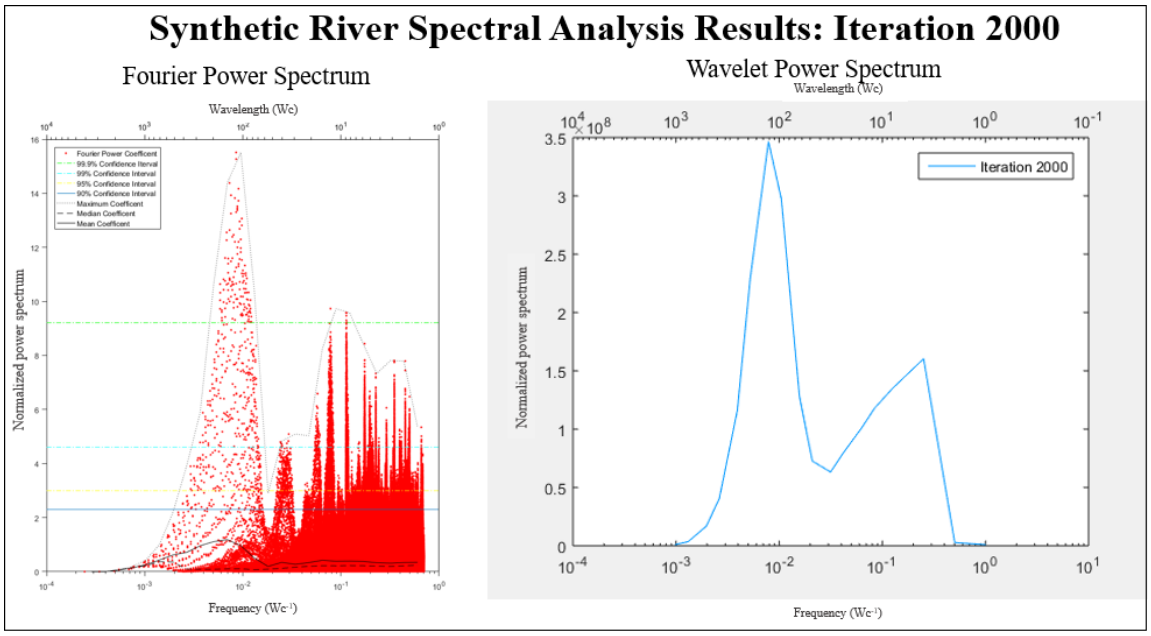

Figure 33. 1D Fourier (left) and wavelet (right) power spectrum for the 2000th synthetic river output

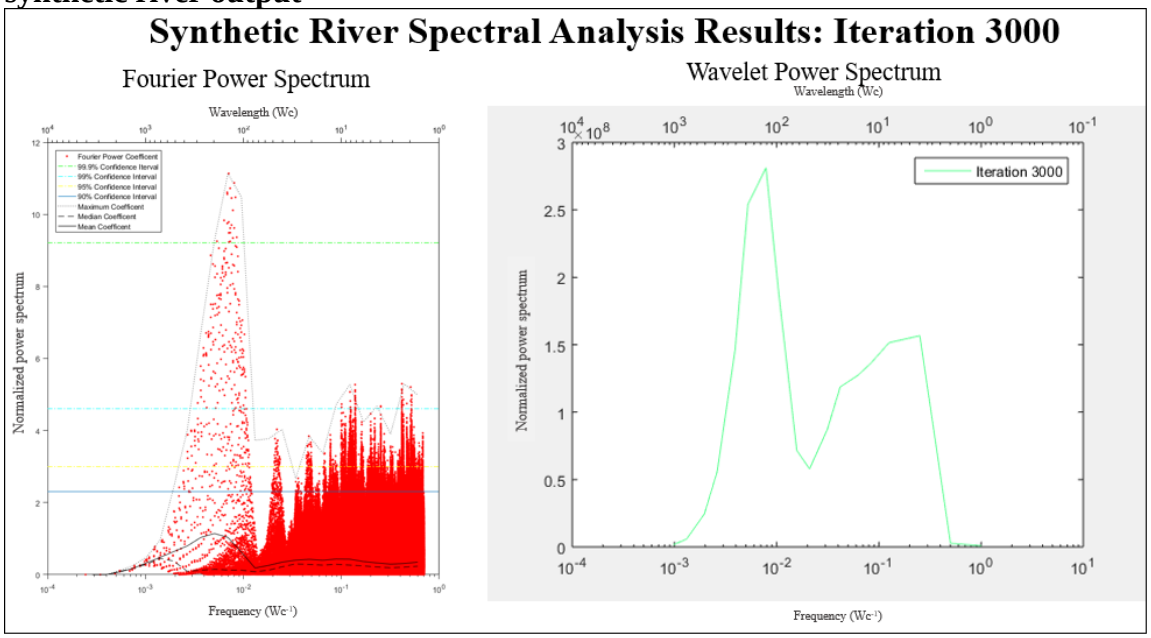

Figure 34. 1D Fourier (left) and wavelet (right) power spectrum for the 3000th synthetic river output

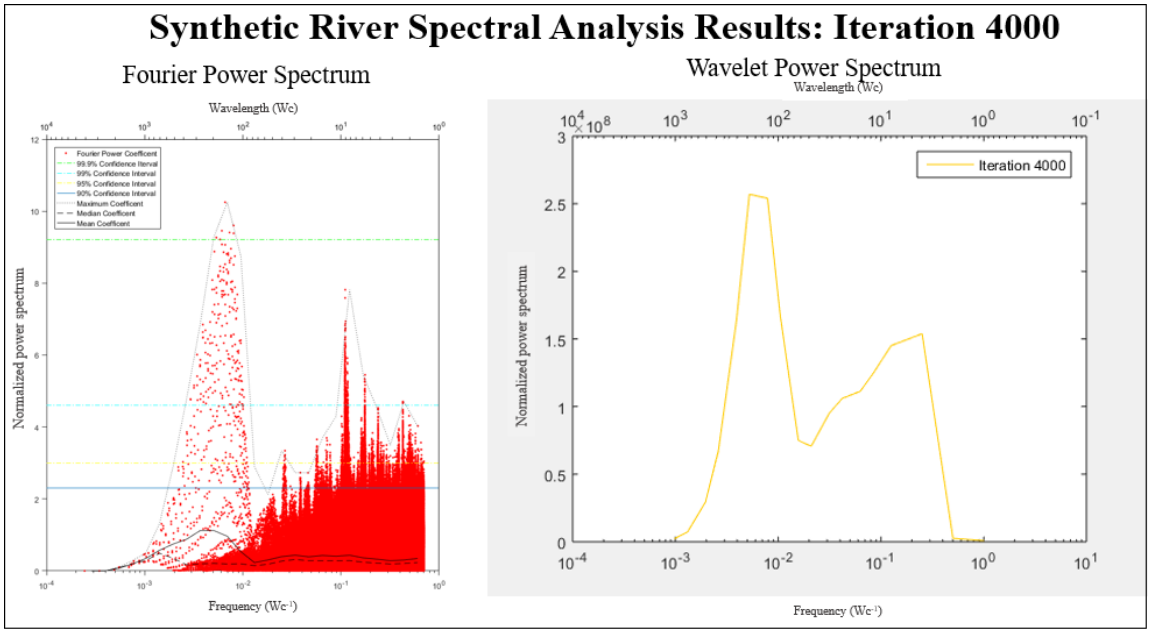

Figure 35. 1D Fourier (left) and wavelet (right) power spectrum for the 4000th synthetic river output

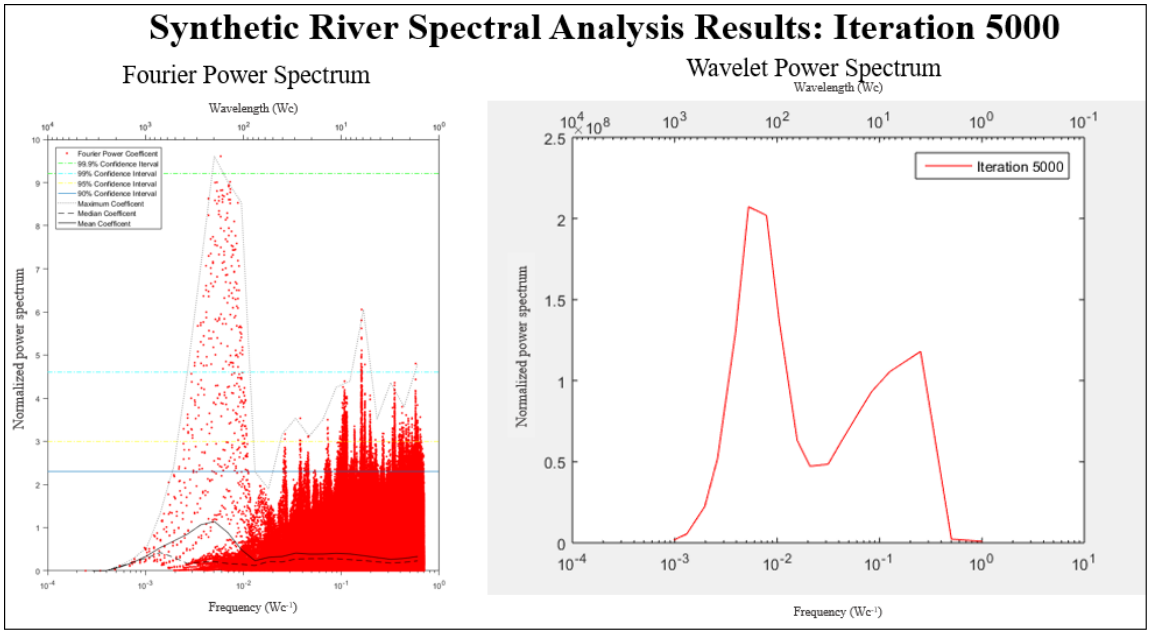

Figure 36. 1D Fourier (left) and wavelet (right) power spectrum for the 5000th synthetic river output

To better understand how the characteristic scale changes over time, we can also visualize the 1D wavelet power spectrum in a single plot (Figure 37). Here, we can see the transformation of the characteristic scales across time. At the beginning, it appears that both types of characteristic scales have about the same amount of power, which seem to indicate a not strongly developed meander feature on the landscape and seems to show that the channel has a large influence on the shape of the landscape than the meander itself. However, this changes as the iterations approach the 2000th iteration, in which the spectral power for the meander-train scale features increases significantly. While the spectral power varies for the meander-train scale features after the 2000th iteration, they remain larger than a particular iteration's bend-scale features.

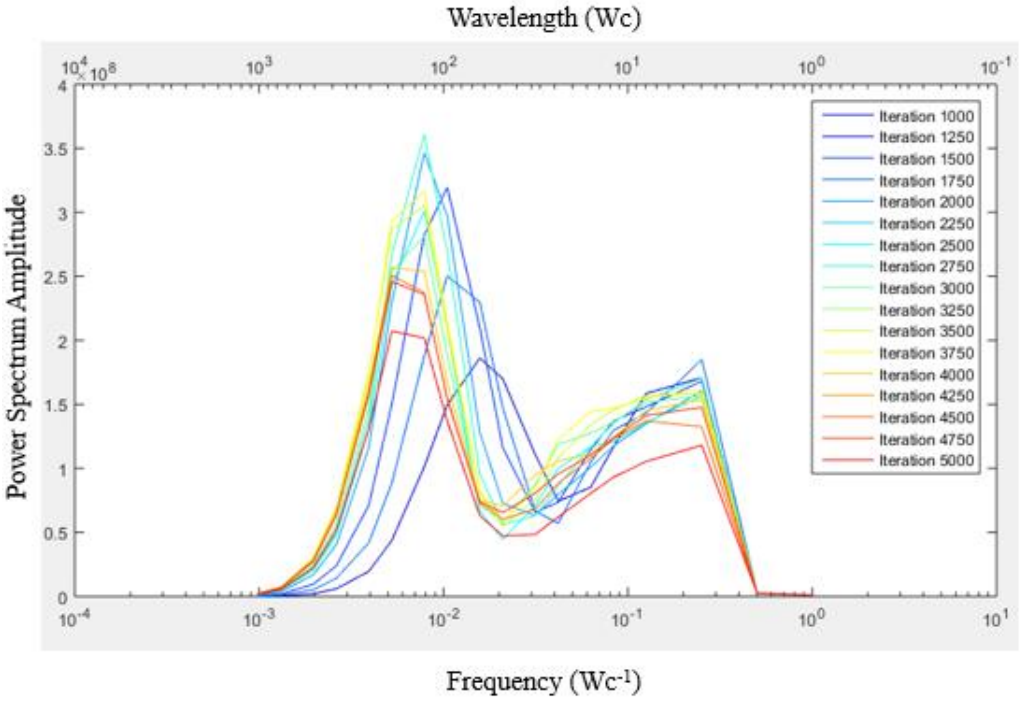

Figure 37. 1D wavelet power spectrum for each river iteration tested

To aid in the visualization of the wavelet spectrum, the 2D power spectrum of the wavelet characteristic scales can also be viewed. Figure 31 to Figure 35 show the 2D power spectrum for the bend-scale and meander-train scale, in addition to showing the corresponding original DEM and the 1D wavelet power spectrum. Here, clear patterns can be seen in where the power spectra is concentrated at each scale range. For the bend-scale power spectrum, typical concentrations in power spectrum range from 5-10 channel widths, and are largely only visible around the channels themselves, those there are weaker concentrations of power near oxbow lakes and meander scars. For the meander-train scale features, the 1000th and 2000th iterations, the power is largely concentrated uniformly throughout the meander. However, at the 3000th iteration, the spectral power at the meander-train scale is concentrated at areas where the river is especially concentrated. Areas along the river that have meanders that seem to bunch up with other meanders tend to have higher spectral power. It seems to be related to areas along the floodplain that are particularly "active" in that the there is much more cutting and depositing of sediments versus other areas within the river. Figures 38 to 42 show the how the floodplain, 1D wavelet spectral power, and the 2D wavelet spectral power changes iteration 1000 to iteration 5000.

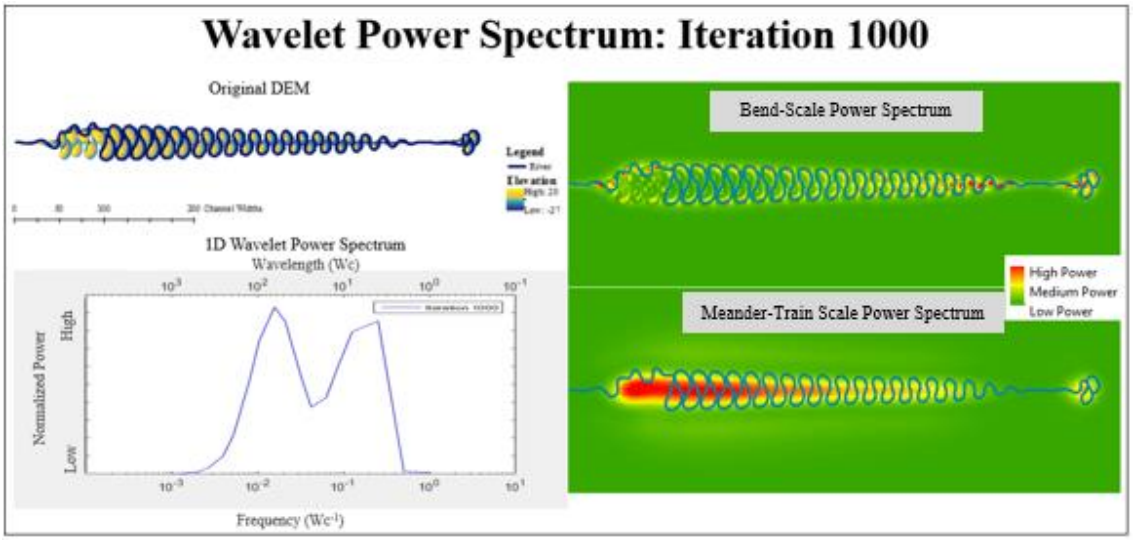

Figure 38. River iteration 1000 with original DEM (upper left), and 1D wavelet power spectrum (lower left), 2D power spectrum for the bend-scale (upper right), and 2D power spectrum for the meander-train scale

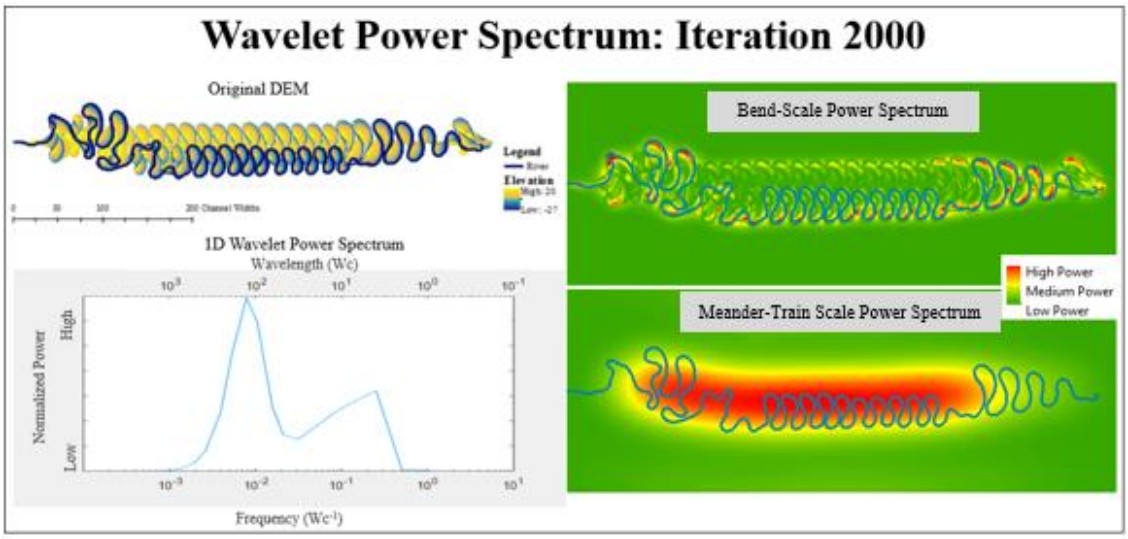

Figure 39. River iteration 2000 with original DEM (upper left), and 1D wavelet power spectrum (lower left), 2D power spectrum for the bend-scale (upper right), and 2D power spectrum for the meander-train scale

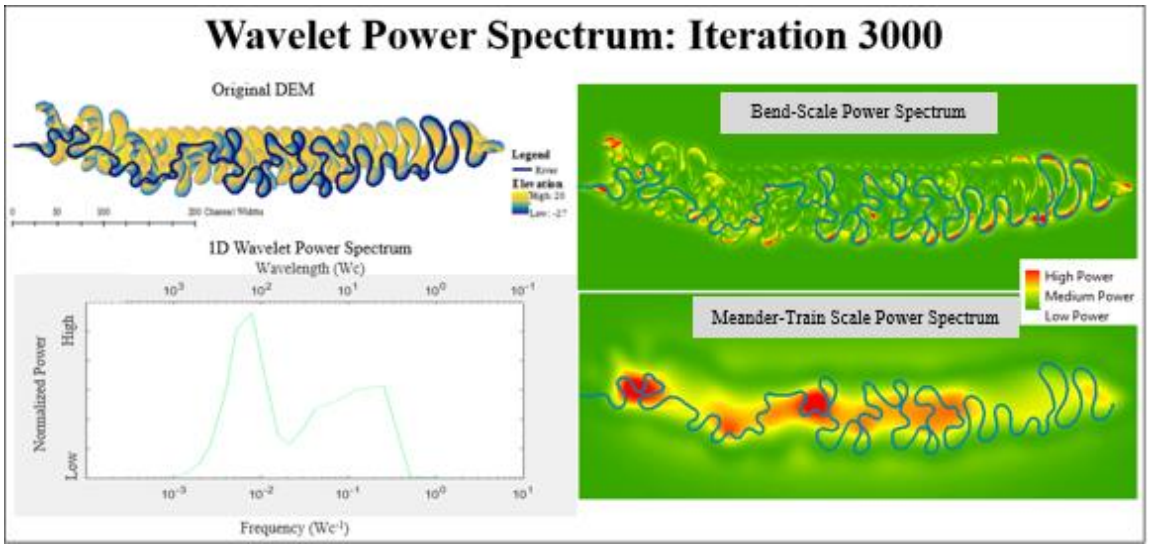

Figure 40. River iteration 3000 with original DEM (upper left), and 1D wavelet power spectrum (lower left), 2D power spectrum for the bend-scale (upper right), and 2D power spectrum for the meander-train scale.

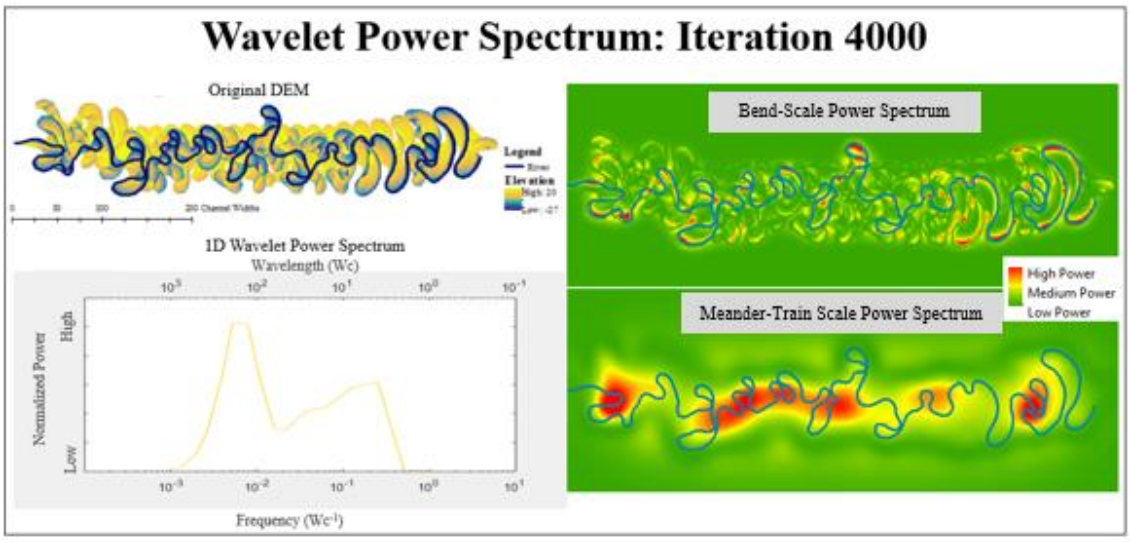

Figure 41. River iteration 4000 with original DEM (upper left), and 1D wavelet power spectrum (lower left), 2D power spectrum for the bend-scale (upper right), and 2D power spectrum for the meander-train scale.

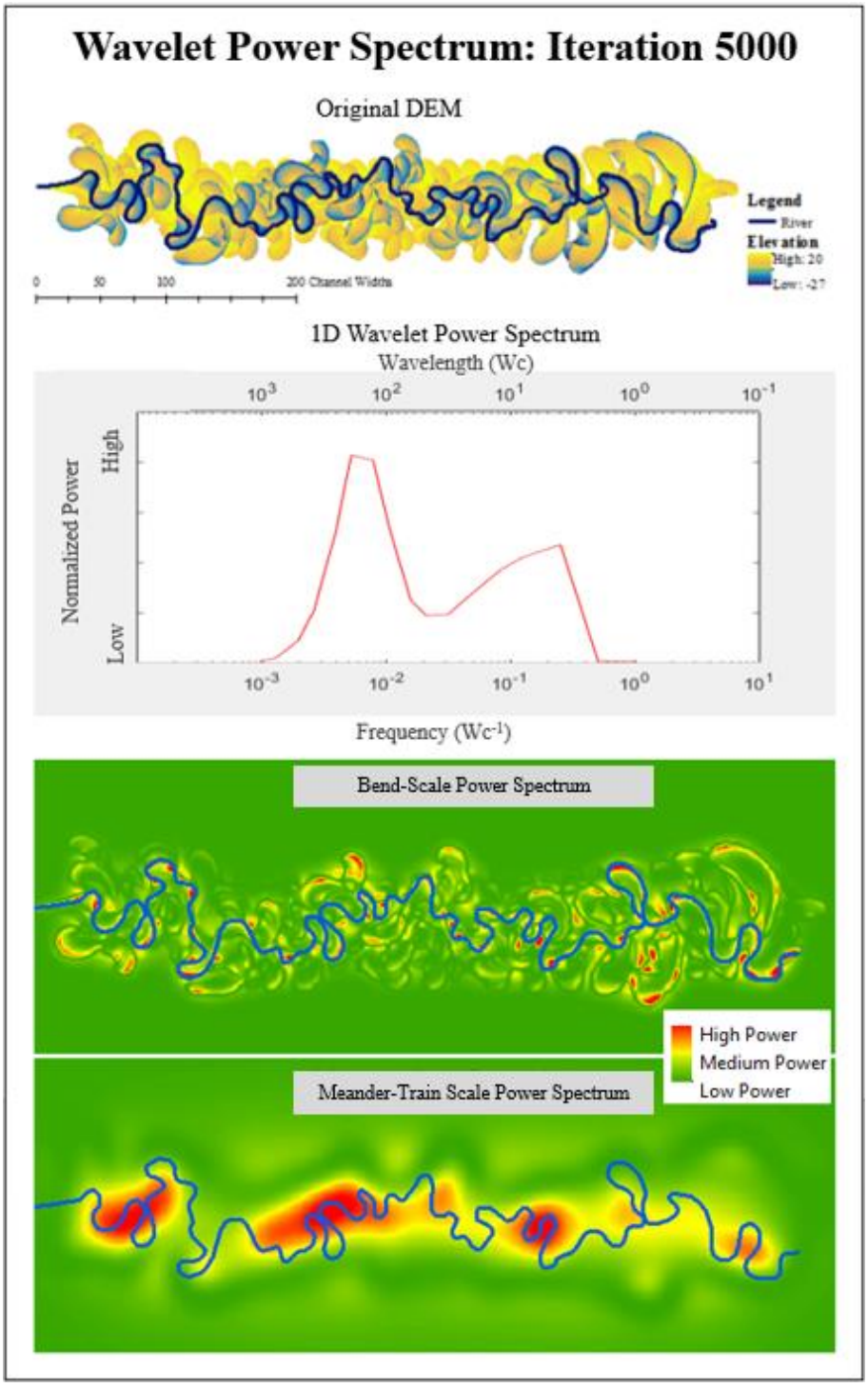

Figure 42. River iteration 5000 with original DEM (upper left), and 1D wavelet power spectrum (lower left), 2D power spectrum for the bend-scale (upper right), and 2D power spectrum for the meander-train scale.

CHAPTER IV

DISCUSSION

4.1 Success of the two algorithms at identifying characteristic scale

Both the Fourier and wavelet algorithms performed largely the same for most test surfaces with small differences. When given a particular surface, if the appropriate background spectrum is used, the results from the Fourier analysis and the wavelet analysis are largely similar to each other, which is clearly seen in the Sine-wave test image result and the fractal surface with and without a characteristic scale. When looking at the global spectrum, it appears that the Fourier analysis is more sensitive to slight changes in the spectrum, versus the wavelet analysis, which appears to give an more generalized result when compared to the Fourier analysis. This could be useful when trying to identify the true range of scales that are appropriate for analysis, though it could potentially hide important results. For instance, while the sine-wave test image, both the 32 unit wavelength feature and the 128 unit wavelength feature are visible in the 1D global Fourier results, though for the 1D global wavelet results, the 32 unit wavelength feature is inundated at a lower signal to noise ratio. There are certain aspects of this test which may have given the Fourier analysis the advantage, the largest being that the Fourier transform is very effective at identifying sine-wave like features in an image, while the Mexican Hat wavelet is designed for Gaussian-like features, and would not be as effective at picking out a sine-wave like feature, especially if it is inundated with noise. However, this test, and the other experiments do bring light for

the 1D global spectrum results that the Fourier analysis may be slightly more sensitive for certain applications such as ...

However, when it comes to the 2D representation of the power spectrum, the wavelet analysis certainly has the advantage, especially at retaining the XY location of the power spectrum so that features can be referenced on the actual image. Conversely, the 2D power spectrum from the Fourier transform displays the power in the frequency domain, which makes it impossible to determine which features are contributing to the power spectrum and where these features exist on the study area.

While the spatial representation of the wavelet power spectrum is useful, it may be difficult to determine how best to display this data. For this thesis, ranges of characteristic scales were identified, and then summed together to present a 2D representation of the spectrum, though there are other ways of viewing this information. Individual power spectrum scales can be viewed, and when viewed alongside the original data or an overlay of the important feature such as a river outline, it becomes much clearer what the power spectrum is corresponding to for a particular scale.

The 3D wavelet power spectrum can also be viewed in a 3D volumetric plot, which is the most revealing of the visualization techniques. Trends in the power spectrum across space and scales can easily be visualized. Many features will be displayed across several scales, though it can be difficult to identify which features within the landscape are associated with each concentration in the power spectrum corresponds to specific features in the landscape.

4.2 Synthetic Floodplain Analysis

4.2.1 Comparing Fourier and wavelet 1D power spectrum for identifying global and local characteristic scales

Both 1D power spectrum for the Fourier analysis and the Wavelet power spectrum appear to show results that support each other. While the scales of range may differ slightly between the Fourier and the wavelet analysis, there appears to be two characteristic scales that can be identified for both of them: the first being typically around scales of ~8 to ~16 channel widths, which is more associated with channel-scale features, the second typically ranging from scales ~64 to ~128 channel widths, which is more associated with meander-scale features. These scales also have variations depending on which iteration of the meandering river surface was used in the analysis. The largest difference between the two spectral analysis techniques is the apartment sensitivity. The Fourier results typically displays more abrupt peaks at smaller wavelength scales in the power spectrum while for wavelet results the peaks appear to be more generalized. The concentration of certain peaks at specific shorter wavelengths could be a response to the discrete nature of the DEM itself, which the Fourier transform would be more sensitive to at shorter wavelengths. In both cases, power spectrum results that are at or below the Nyquist frequency do not necessary portray accurate results (Perron, Kirchner, and Dietrich 2008).

4.2.2 1D Power Spectrum across meandering river floodplain iterations

The data used for the floodplain analysis was created using the model by Howard (1996), and uses progressive iterations of the river floodplain to generate the next

meandering river floodplain surface as if over a time-series. So the 1000th iteration of the meandering river floodplain would represent a younger meandering river floodplain versus the 5000th iteration of the meandering river floodplain. For this analysis, iterations 1000 to 5000 were observed, using 250 iterations time-steps. From this, patterns of the differences in the 1D power spectrum can easily be identified. Table 1 shows how the shifts in local and global characteristic scales change over time. Throughout all iterations, there are clearly two major characteristics scales: a dominant characteristic scale which is associated with meander-scale features, and a local characteristic scale is associated with smaller, channel-scale features. Beginning at 1000 iterations, the difference in magnitude between the meander-scale features and the channel-scale features is not very large, and the range of scales are closer together. As time progresses, the meander-scale features gain a large amount of spectral power, meaning that they have a larger dominance over the landscape than the bend-scale features, though this increase in spectral power for the meander-train scale features begins to decrease around 3000th iteration. In addition, the range of scales for the two characteristic scales begins to drift apart.

This pattern illuminates the ability of this algorithm to potentially be used to determine the age or state of a meandering river floodplain. When a meandering river floodplain is younger, the bend-scale features have as much influence on the overall landscape as the meander-train scale features. As the meander river floodplain ages and river has more time to influence the floodplain, the meander-train scale features and

more long-term topographic influences on the landscape become more dominant in contrast to the topographic effects of the channel.

4.2.3 2D wavelet power spectrum qualitative analysis

The 2D wavelet power spectrum for each scale, over the 2D Fourier power spectrum, allows for visualization of the XY location of the concentration of power for a particular scale. Once the range of scales that are associated with a characteristic scale range are identified with the 1D wavelet power spectrum, the scale's power spectrum can be summed to compute a 2D wavelet power spectrum which highlights where characteristic features exist in a landscape. In this study, for each iteration, two of these surfaces were created, the first for the characteristic scales that were associated with bend-scale features and the second for the characteristic scales associated with meander-train scale features.

For meander-train scale features, it largely appears that concentrations of power occur in locations that have a high amount of clustering in the river itself, that is, areas where multiple meanders are very close to each other. In Figure 42 for the 5000th iteration, this can clearly be seen at the three locations where clustering of meander bends appears to be higher. As we progress backwards through the iterations, this same pattern tends to hold. Although we are observing the 1000th and 2000th iterations, this pattern appears to be more uniform throughout the landscape, and seems to have uniform spectral power throughout the floodplain. It appears that because most of these areas have a more consistent level of clustering. It is also important to note that the overall spectral power for the meanders scale features for the earlier iterations around 1000

iterations to 2000 iterations do not have a particularly strong spectral power response at these scales when compared to later iterations around 3000 to 5000 iterations. It appears that spectral power response may be related to a measure of activity within the meander river floodplain.

At the bend-scale features, features that appear to be actively cutting or depositing sediments on the floodplain appear to how the stronger spectral response. While the hotspots for spectral power for the meander-train scale feature appear to range from 25 to 50 channel widths, the hotspots for the bend-scale features appear to be around 5 to 10 channel widths in size, and typically appear directly next to the river itself, or recently created oxbows. Though more rigorous testing which is outside of the scope of this thesis must be done in order to definitely demonstrate this relationship, the characteristic scale for the bend-scale features does appear to correspond to geophysical processes of the meandering river on the floodplain.

4.2.4 2D wavelet power spectrum quantitative analysis: surface metrics relationships

To better quantitatively assess what aspects of the meandering river floodplain that the spectral analysis was highlighting, the 2D spectral power at the characteristic meander-train scale and characteristic bend-scale features were compared to surface metrics which are commonly used to assess different topographic features of floodplains (Scown, Thoms and De Jager 2015). These metrics included focal mean (Nogami 1995, Gadelmawla et al. 2002), rugosity (Nogami 1995, Hakkinen, Makinen and Coley 1986), range (Nogami 1995) , standard deviation of the elevation (Gadelmawla et al. 2002), standard deviation of the curvature (McCormick 1994), coefficient of variance

(McCormick 1994), volume area ratio (Nogami 1995), and texture (Scown et al. 2015, Iwasaki, Shimizu and Kimura 2013). All of these metrics rely on a circular sliding window technique to generate the results. These surface metrics were computed using a window size of 25 channel widths, which corresponds approximately to half of the smallest scale which corresponded to the meander-train scale characteristic features, or the radius of the wavelet scale, and is also the typical size of the power spectrum hotspots for this scale range. Stratified samples every 50 by 50 pixels were extracted and used to determine the possibility of a relationship between the power spectrum and the surface metrics to consistently sample each of the power spectrum results. The regression equations and the R-squared values that were generated can be seen in Table 2. Of all the eight surface metrics used in this assessment, focal mean and rugosity show the strongest relationship. Figure 43 and Figure 44 show the regressions.

Table 2. R-squared values for relationship between surface metric and power spectrum

	Bend-scale Regression R-square		**Meander-train scale Regression R-square**	
Surface Metric	**Linear Regression**	**Third-degree Polynomial Regression**	**Linear Regression**	**Third-degree Polynomial Regression**
Focal Mean	0.4949	0.56	0.7149	0.799
Rugosity	0.4765	0.5132	0.7031	0.801
Standard Deviation (curvature)	0.2928	0.3245	0.4192	0.4921
Coefficient of Variation	0.3807	0.3298	0.4733	0.5886
Volume Area Ratio	0.0214	0.0227	0.0058	0.0324
Texture	0.2218	0.2754	0.2218	0.2754
Standard Deviation (elevation)	0.2273	0.2847	0.2686	0.3988
Range	0.292	0.3897	0.2142	0.2875

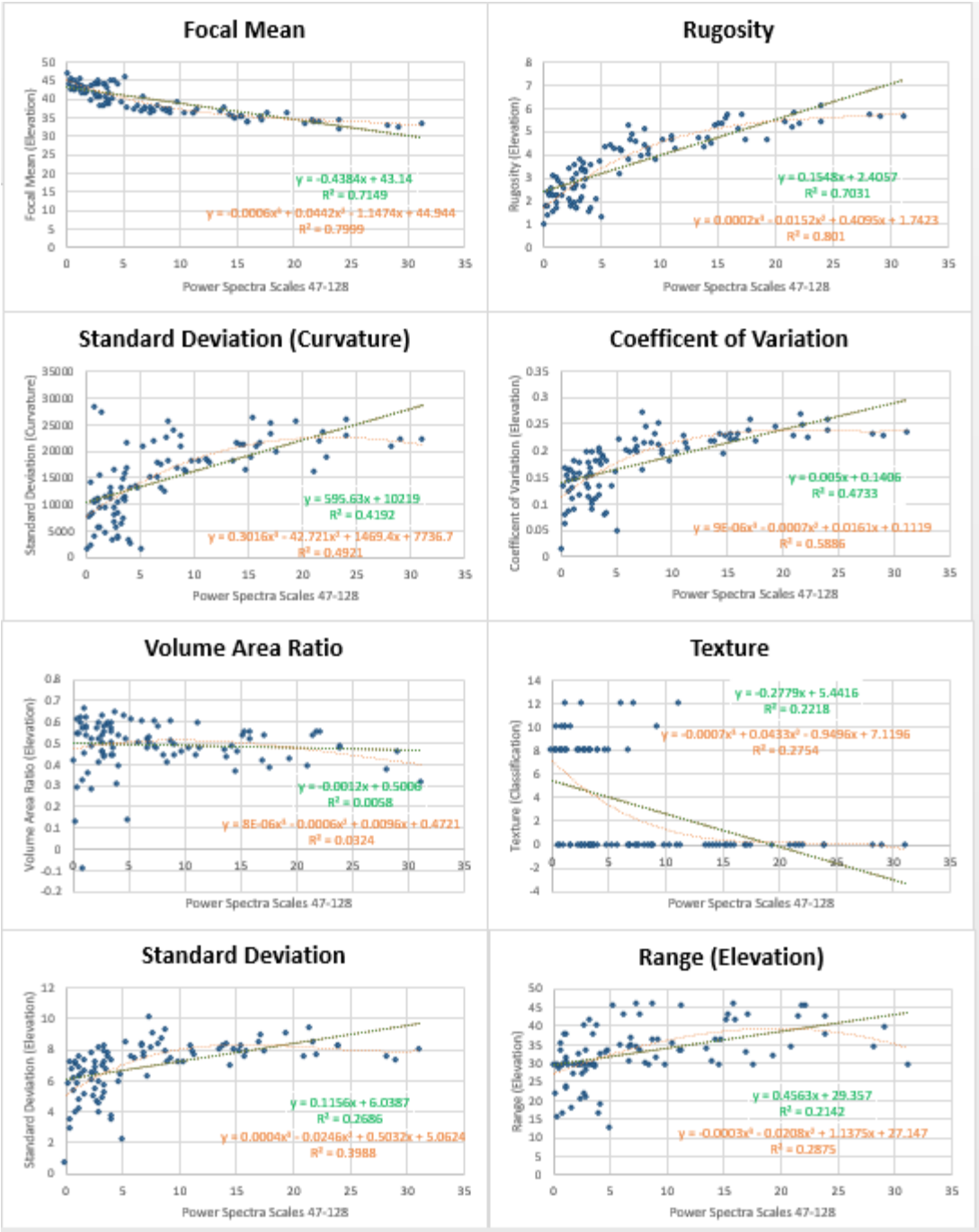

Figure 43. Regression plots showing the relationship of surface metrics to the power spectrum (Meander-train scale power spectrum versus surface metrics of 25 Wc window size)

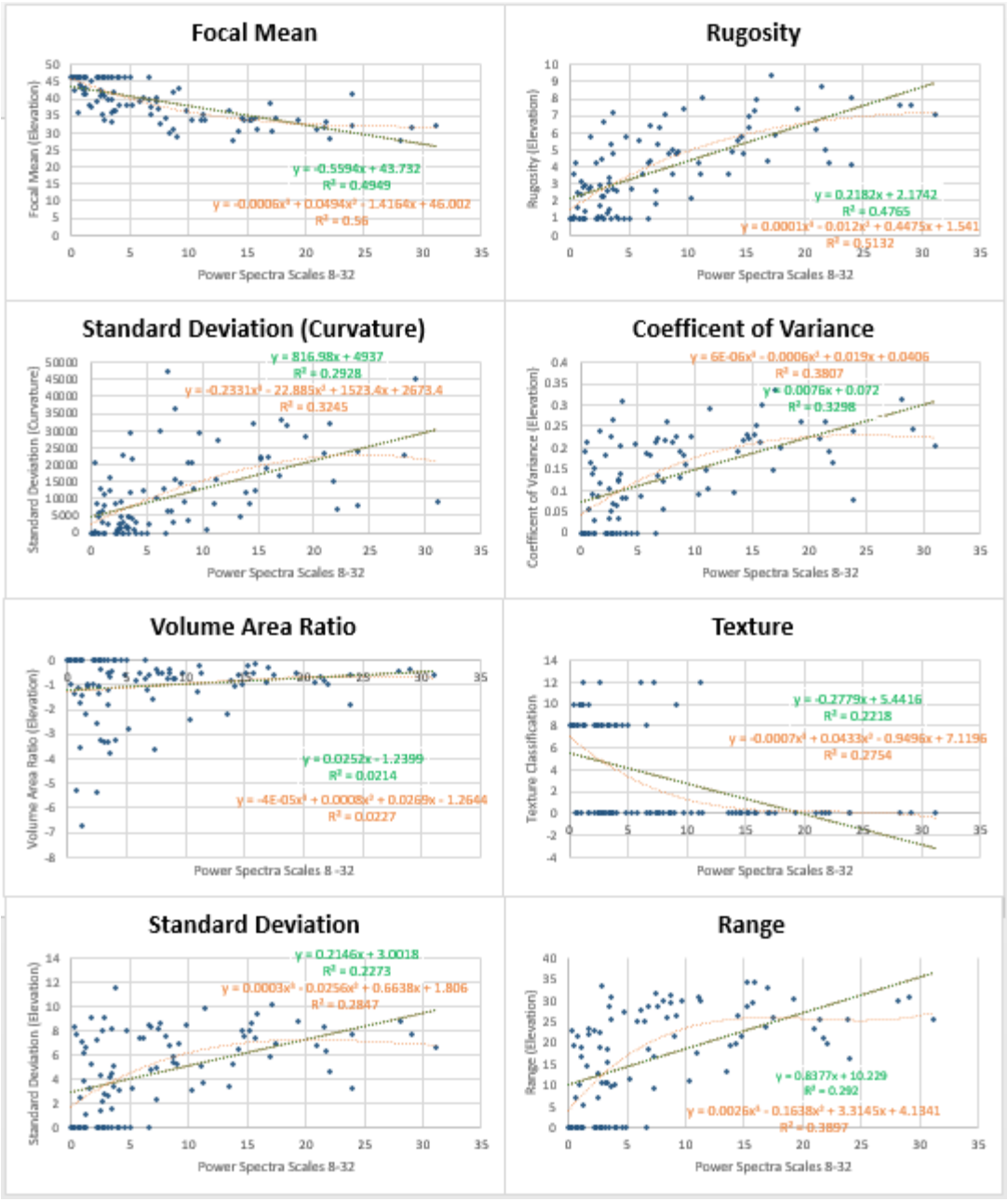

Figure 44. Regression plots showing the relationship of surface metrics to the power spectrum (Bend-scale power spectrum versus surface metrics of 5 Wc window size)

This relationship could be explained with mathematical relationship between a wavelet and the surface metrics focal mean and rugosity. A wavelet transform could be

thought of fitting a particular waveform to an image. The relationship between the power spectrum and rugosity at this scale seems to have a reasonable explanation, in that rugosity has been shown to be related convolutedness of a surface and can serve as an indicator of a major structuring processes on the meandering river floodplain.

The relationship with focal mean would also seem reasonable, as a wavelet scale increases, the amplitude of the wavelet increases. Although something that is unexpected with this particular dataset is that as spectral power at the meander-train scale increases, the focal mean decreases. Areas along the meandering river floodplain that have a lower elevation are areas in which meander-river channels have experienced more cutting. This indicates that the wavelet power spectrum is not just detecting the amplitude of elevation but the structure of the meandering river floodplain at this particular scale.

Similar surface metrics to rugosity that measure surface showed weaker relationships to the power spectrum. Standard deviation of elevation, standard deviation of curvature and coefficient of variation show weaker relationships with an R-squared around 0.4.

Rugosity could possibly be showing a stronger correlation to spectral power because unlike the other surface metrics for roughness, it is better able at measuring structural characteristics of an area versus measuring the variation. The high correlation between rugosity and focal mean indicate the wavelet power spectrum at certain scales could be used to reveal structural components at the meander-train scale.

For the bend-scale features, the same metrics were used, though a window size of 5 channel widths was used. For this, focal mean and rugosity also showed to have the

strongest correlation to spectral power, though the relationship was much weaker with an R-squared value around 0.5. Further testing will be required to more definitively identify the cause for this weak relationship.

4.3 Contribution and significance to the field of spectral analysis in geoscience applications

While spectral analysis techniques to better understand geophysical processes or landscapes is not necessarily new, this work takes a very commonly used 1D continuous wavelet analysis methodology that is outlined in previous proponent papers (Torrence and Compo 1998, Bradshaw and Spies 1992, Mount et al. 2013, Zolezzi and Güneralp 2016) and implements those on a 2D data using a 2D continuous wavelet analysis. Namely, this work underlines the importance of establishing a theoretical background spectrum to conduct proper spectral analysis of landscapes. Other works which have tried to use spectral analysis for landscapes did not assign a background spectrum (Kalbermatten et al. 2012). While for certain landscapes or types of data, scales could be identified that could be considered characteristic, it would be difficult to make the methodology ubiquitous to other landscapes which do not share similar properties. Establishing a proper background spectrum for analyzing landscapes allows for an endless variety of landscapes to be analyzed.

In addition, to our knowledge, this study presents the first application of 2D spectral analysis on a meandering river floodplain. While similar work has been done on DEMs of drainage basins (Perron, Kirchner and Dietrich 2008), or spectral analysis on a

meandering river planform (Zolezzi and Güneralp 2016), it had yet to be done on a meandering river floodplain.

The significance of this work goes beyond testing a new algorithm on a meandering river floodplain, however. Through identifying the characteristic scale of synthetic meandering river floodplains, and examining the results against other surface metrics, the findings suggest that the power spectrum from 2D wavelet analysis at certain scales may be related to the geophysical processes of the meandering river and not just the topographic nature of a meandering river floodplain, which shows that 2D spectral analysis can potentially be used to identify particular geophysical processes giving rise to particular landscape features. With further research, this could lead to algorithms which can determine more than just the characteristic scale of a fluvial river floodplain, but also the geophysical processes of a particular floodplain at specific locations.

CHAPTER V

FUTURE WORK AND CONCLUSION

5.1 Future Work

5.1.1 River Floodplain Analysis

This thesis research was able to identify the characteristic scale of a synthetic meandering river. However, this research has also prompted other questions which may warrant further research in the future, both in regards to the algorithms used in this thesis as well as analysis of meandering river floodplains.

5.1.1.1 Experiments with different resolutions, parameters, and real world DEMs

Further investigation into different types of river meanders may reveal different types of information about a river. For the experiments for this thesis, it was clear that as the river aged over time that the global power spectrum changed, as well as the location of where the power spectrum was concentrated. All of these surfaces were created via the Howard Model and were progressive iterations of the river floodplain. Running a similar set of experiments on the same river with different input parameters to the Howard Model may reveal different types of information. Also, increasing the spatial resolution of the output synthetic DEMs would allow for accurate spectral analysis at smaller scales. For this thesis, the DEMs has a pixel resolution of 1 channel width. A higher resolution DEM would allow for potential identification of patterns that would for this thesis not be possible to retrieve in these experiments.

Though reaching a solid understanding of how this algorithm behaves with synthetic data is important, the eventual goal is to be able to use this algorithm for analysis on a DEM of a true meandering river floodplain.

5.1.1.2 Wavelet comparison to geomorphic landforms

For this thesis, the wavelet power spectrum results were compared to surface metrics to help relate the power spectrum results to other landscape characteristics. However, this provides a limited information as to what the power spectrum is related at specific scales. Classifying a meandering river floodplain by its landscape features such as "point bars" and "meander scars" and then comparing this to the wavelet power spectrum at different characteristic scales may reveal more information content. Qualitatively, it appears that the spectral power at the characteristic scales ~50 river channel widths to ~150 is related to a high density of meandering cutting features. This relationship can only truly be verified with a quantitative analysis. Future work will use landscape features to examine the relationship of meandering river floodplain features to the power spectrum.

5.1.1.3 Meandering river floodplain classification

It is clear that the power spectrum at different scales tends to identify different types of features, with small scale features identifying bend-scale features such as smaller cuts or areas along the floodplain that deposit sediments and larger scales identify mesomorph features. Since different size scales are able to detect different categories of features, it appears that the power spectra at different scales could be used as inputs to a classification algorithm. While there has been other works which have

used the power coefficients for image classification (Zhang et al. 2011), there seems to be limited work for this particular methodology in using the power spectrum of DEMs to classify different landforms, especially for meandering river floodplains.

5.1.2 Future enhancements to methodology

5.1.2.1 Wavelet analysis in the Fourier spectrum

The wavelet transform can be implemented on the data in the spatial domain or the frequency domain (Cooley and Tukey 1965). Even if the results are computed in different domains, provided that the same wavelet and scales are used, the wavelet coefficients would achieve the same result. For this thesis, the spatial variant of the continuous wavelet transform was used similar to the way it was used in the literature. However, using the frequency domain variant may increase the speed of the continuous wavelet transform algorithm.

5.1.2.2 Analytic generation of theoretical background noise

The algorithms provided were able to provide the desired results and work as a proof of concept that the wavelet analysis is an effective tool. Although using a numeric solution for generating a background spectrum is capable of providing accurate results, it can very time-consuming with small scenes taking several minutes, and larger scenes taking several hours or days. An analytical solution as outlined in Chapter I Section 1.5.4.3 if implemented correctly may increase the speed, especially for larger images. In addition, because the red noise would be calculated analytically, the precise theoretical background red noise spectrum could easily be applied, versus using a generic white,

pink, or red noise surface, or by estimating the red noise based on a numerical approach. This would allow for faster generation of accurate results.

5.1.2.3 Increasing use ability for more widespread use

Torrence and Compos (1998) created a robust framework to analyze 1D signals using the continuous wavelet transform. By showing scientists how the algorithm works and providing scripts in an easy to use format in addition to providing visualization techniques which can be widely utilized, their work has had a very large impact. While they are not the ones to create this form of analysis, the tools they developed helped bring spectral analysis to the forefront of geoscience research. However, they do not extend this to the 2D analysis. There are several major challenges to 2D continuous wavelet analysis versus 1D continuous wavelet analysis. The first being that with a 1D CWT, the input is a 1D signal but the output is a 2D array of power coefficients. For a 2D input in the 2D CWT, the result is a 3D cube of power coefficients. This is obviously much more difficult to analyze and interpret. This work has demonstrated several different ways that this can be done in 1D and 2D, in addition to exploring different visualization techniques of the 3D power spectrum cube to garner more information.

5.2 Synthesis and Conclusion

This work has shown 2D spectral analysis can be effectively used to identify characteristic scale in a 2D array or DEM. This goes both for the Fourier transform and wavelet analysis. However in either case, this work highlights the importance of selecting the appropriate background spectrum in order to perform effective analysis.

The methods outlined in this paper were both able to identify a range of scales for synthetic images that could be identified as characteristic to a specific area, and once identified, could be related to the features in the original dataset which they are related.

REFERENCES

Abad, J. & M. Garcia (2009) Experiments in high-amplitude Kinoshita meandering channel: 1. Implication of bend orientation on mean and turbulent flow structure. *Water Resources Research,* 45.

Addisson, P. 2004. *The Illustrated Wavelet Transform Handbook*. Bristol, U. K.: Inst. of Phys. Publ.

Ahnert, F. (1984) Local Relief and the Height Limits of Mountain Ranges. *American Journal of Science,* 284**,** 1035-1055.

Antonie, J., R. Murenzi, P. Vandergheynst & T. S. 2004. *Two-Dimensional Wavelets and Their Relatives*. Cambridge, U. K.: Cambridge Univ. Press.

Balmino, G. (1993) The Spectra of the Topography of the Earth, Venus, and Mars. *Geophysical Research Letters,* 20**,** 1063-1066.

Baschin, O. (1916) The Origin of the River Meanders. *Petermanns Mitteilungen,* 62**,** 16-16.

Bedient, P. B. & W. C. Huber. 2002. *Hydrology and Floodplain Analysis*. Upper Saddle River, NJ: Prentice Hall.

Blackman, R. B. & J. W. Tukey. 1958. *The Measurement of Power Spectra*.

Booth, A. M., J. J. Roering & J. T. Perron (2009) Automated landslide mapping using spectral analysis and high-resolution topographic data: Puget Sound lowlands, Washington, and Portland Hills, Oregon. *Geomorphology,* 109**,** 132-147.

Bradshaw, G. A. & T. A. Spies (1992) Characterizing canopy gap structure in forests using wavelet analysis. *Journal of Ecology,* 80**,** 205-215.

Brown, R. A., G. B. Pasternack & W. W. Wallender (2014) Synthetic river valleys: Creating prescribed topography for form-process inquiry and river rehabilitation design. *Geomorphology,* 214**,** 40-55.

Bruun, B. T. & S. Nilsen (2003) Wavelet representation of large digital terrain models. *Computers & Geosciences,* 29**,** 695-703.

Caswell, H. & J. E. Cohen (1995) Red, White, and Blue - Environmental Variance Spectra and Coexistence in Metapopulations. *Journal of Theoretical Biology,* 176**,** 301-316.

Catano-Lopera, Y. A., J. D. Abad & M. H. Garcia (2009) Characterization of bedform morphology generated under combined flows and currents using wavelet analysis. *Ocean Engineering,* 36**,** 617-632.

Cooley, J. W. & J. W. Tukey (1965) An Algorithm for the Machine Calculation of Complex Fourier Series. *Mathmatics of Computation,* 19**,** 297-301.

Crave, A. & P. Davy (1997) Scaling relationships of channel networks at large scales: Examples from two large-magnitude watersheds in Brittany, France. *Tectonophysics,* 269**,** 91-111.

Davis, W. M. (1905) The geographical cycle in an arid climate. *Journal of Geology,* 13**,** 381-407.

--- (1913) Meandering Valleys and Underfit Rivers. *Annals of the Association of American Geographers,* 3**,** 3-28.

Dodds, P. S. & D. H. Rothman (2000) Scaling, universality, and geomorphology. *Annual Review of Earth and Planetary Sciences,* 28**,** 571-610.

--- (2001) Geometry of river networks. I. Scaling, fluctuations, and deviations. *Physical Review E,* 63.

Fournier, A., D. Fussell & L. Carpenter (1982) Computer rendering of stochastic models. *Communications of the ACM,* 25**,** 371-384.

Gadelmawla, E. S., M. M. Koura, T. M. A. Maksoud, I. M. Elewa & H. H. Soliman (2002) Roughness parameters. *Journal of Materials Processing Technology,* 123**,** 133-145.

Gallant, J. C. & M. F. Hutchinson (1997) Scale dependence in terrain analysis. *Mathematics and Computers in Simulation,* 43**,** 313-321.

Gilbert, G. K. (1909) The convexity of hilltops. *Journal of Geology,* 17**,** 344-350.

Gilbert, L. E. (1989) Are Topographic Data Sets Fractal. *Pure and Applied Geophysics,* 131**,** 241-254.

Gilman, D. L., F. J. Fuglister & J. M. Mitchell (1963) On the power spectrum of red noise. *Journal of the Atmospheric Sciences,* 20**,** 182-184.

Güneralp, I. & R. Martson (2012) Process-form linkages in meander morphodynamics: Bridging theoretical modeling and real world complexity. *Progress in Physical Geography,* 36.

Hakkinen, J. S. R. K. I., Y. Makinen & P. N. M. P. P. Coley (1986) River dynamics and the diversity of Amazon lowland forest. *Nature,* 332**,** 254-258.

Horton, R. E. (1932) Drainage-basin characteristics. *Transactions-American Geophysical Union,* 13**,** 350-361.

--- (1945) Erosional Development of Streams and their Drainage Basins - Hydrophysical Approach to Quantitative Morphology. *Geological Society of America Bulletin,* 56**,** 275-370.

Hovius, N. (1996) Regular spacing of drainage outlets from linear mountain belts. *Basin Research,* 8**,** 29-44.

Howard, A. D. 1996. Modelling Channle Evolution and Floodplain Morphology. In *Floodplain Processes,* eds. M. G. Anderson, D. E. Walling & P. D. Bates, 15-62. Chichester: John Wiley & Sons.

Ijjaszvasquez, E. J., I. Rodriguez-Iturbe & R. L. Bras (1992) On the Multifractal Characteristization of River Basins. *Geomorphology,* 5**,** 297-310.

Iwasaki, T., Y. Shimizu & I. Kimura (2013) Modelling of the initiation and development of tidal creek networks. *Proceedings of the Institution of Civil Engineers-Maritime Engineering,* 166**,** 76-88.

Kaiser, G. 1994. *A Friendly Guide to Wavelets*. Boston: Birkhauser.

Kalbermatten, M., D. Van De Ville, P. Turberg, D. Tuia & S. Joost (2012) Multiscale analysis of geomorphological and geological features in high resolution digital elevation models using the wavelet transform. *Geomorphology,* 138**,** 352-363.

Kumar, P. & E. Foufoula-Georgiou (1997) Wavelet analysis for geophysical applications. *Reviews of Geophysics,* 35**,** 385-412.

Labarbera, P. & R. Rosso (1989) On the Fractal Dimension of Stream Networks. *Water Resources Research,* 25**,** 735-741.

Labat, D. (2005) Recent advances in wavelet analyses: Part 1. A review of concepts. *Journal of Hydrology,* 314**,** 275-288.

Labat, D., J. Ronchail & J. L. Guyot (2005) Recent advances in wavelet analyses: Part 2 - Amazon, Parana, Orinoco and Congo discharges time scale variability. *Journal of Hydrology,* 314**,** 289-311.

Lennon, J. J. (2000) Red-shifts and red herrings in geogrpahical ecology. *Ecography,* 23**,** 101-113.

Leopold, L. B., M. G. Wolman & J. P. Miller. 1995. *Fluvial Processes in Geomorphology*. Mineola, New York: Dover Publications.

Mack, C. A. (2011) Analytic form for the power spectral density in one, two, and three dimensions. *Journal of Micro/Nanolithography, MEMS, and MOEMS,* 10.

Mandelbrot, B. B. (1975) Stochastic models for the Earth's relief, the shape and the fractal dimension of the coastlines, and the number-area rule for islands. *Proceedings of the National Academy of Sciences of the United States of America,* 72**,** 3825-3828.

Mark, D. M. & P. B. Aronson (1984) Scale-Dependent Fractal Dimensions of Topographic Surfaces - An Empirical-Investigation, with Applications in Geomorphology and Computer Mapping. *Journal of the International Association for Mathematical Geology,* 16**,** 671-683.

Massel, S. R. (2001) Wavelet analysis for processing of ocean surface wave records. *Ocean Engineering,* 28**,** 957-987.

Matsushita, M. & S. Ouchi (1989) On the Self-Affinity of Various Curves. *Physica D,* 38**,** 246-251.

McCormick, M. I. (1994) Comparison of field methods for measuring surface topography and their associations with a tropical reef assemblage. *Marine Ecology Progress Series,* 112**,** 87-96.

Meyers, S. R. (2012) Seeing red in cyclic stratigraphy: Spectral noise estimation for astrochronology. *Paleoceanography,* 27.

Mitchell, J. M. (1964) Further Remarks on the Power Spectrum of Red Noise. *Journal of the Atmospheric Sciences,* 21**,** 461-461.

Montgomery, D. R. & W. E. Dietrich (1992) Channel Initation and the Problem of the Landscape Scape. *Science,* 255**,** 826-830.

Mount, N. J., N. J. Tate, M. H. Sarker & C. R. Thorne (2013) Evolutionary, multi-scale analysis of river bank line retreat using continuous wavelet transforms: Jamuna River, Bangladesh. *Geomorphology,* 183**,** 82-95.

Newman, W. I. & D. L. Turcotte (1990) Cascade Model for Fluvial Geomorphology. *Geophysical Journal International,* 100**,** 433-439.

Nikora, V. I. (1991) Fractal Structures of River Plan Forms. *Water Resources Research,* 27**,** 1327-1333.

Nogami, M. (1995) Geomorphometric measures for digital elevation models. *Z. Geomorphol. Suppl.,* 101**,** 53-67.

Orloff, T., M. Kreslavsky & E. Asphaug (2013) Distribution of polygon characteristic scale in Martian patterned ground terrain in the northern hemisphere using the Fourier transform. *Journal of Geophysical Research E: Planets,* 118**,** 1558-1566.

Percival, D. B. & A. T. Walden. 1993. *Spectral Analysis for Physical Applications*. New York: Cambridge University Press.

Perron, J. T., J. W. Kirchner & W. E. Dietrich (2008) Spectral signatures of characteristic spatial scales and nonfractal structure in landscapes. *Journal of Geophysical Research: Earth Surface,* 113.

Priestley, M. B. 1981. *Spectral Analysis and Time Series*. New York: Academic Press.

Sayles, R. S. & T. R. Thomas (1978) Surface-Topography as a Nonstationary Random Process. *Nature,* 271**,** 431-434.

Scown, M. W., M. C. Thoms & N. R. De Jager (2015) Measuring floodplain spatial patterns using continuous surface metrics at multiple scales. *Geomorphology,* 245**,** 87-101.

Southworth, R. 1960. Autocorrelation and spectral analysis. In *Mathematical Methods for Digital Computers,* eds. A. Ralston & H. S. Wilf, 213-220. New York: John Wiley & Sons Inc.

Speight, J. G. (1965) Meander Spectra of the Angabunga River. *Journal of Hydrology* 3**,** 1-15.

Stolum, H. H. (1996) River meandering as a self-organization process. *Science,* 271**,** 1710-1713.

Talling, P. J., M. D. Stewart, C. P. Stark, S. Gupta & S. J. Vincent (1997) Regular spacing of drainage outlets from linear fault blocks. *Basin Research,* 9**,** 275-302.

Tary, J. B., R. H. Herrera, J. Han & M. van der Baan (2014) Spectral estimation—What is new? What is next? *Reviews of Geophysics***,** n/a-n/a.

Torrence, C. & G. P. Compo (1998) A Practical Guide to Wavelet Analysis. *Bulletin of the American Meteorological Society,* 79**,** 61-78.

Turcotte, D. L. (1987) A Fractal Interpretation of Topography and Geoid Spectra on the Earth, Moon, Venus, and Mars. *Journal of Geophysical Research-Solid Earth and Planets,* 92**,** E597-E601.

Valenzuela, V. V., R. D. Lins & H. M. De Oliveira. 2013. Application of enhanced-2D-CWT in topographic images for mapping landslide risk areas. In *10th International Conference on Image Analysis and Recognition, ICIAR 2013,* 380-388. Povoa do Varzim.

Voss, R. F. 1988. *Fractals in nature: from charaterisation to simulation*. Springer.

Wang, N. & C. Lu (2009) Two-Dimensional Continuous Wavelet Analysis and Its Application to Meteorological Data. *Journal of Atmosphereic and Oceanic Technology,* 27**,** 652-666.

Ward, F. & R. Sharpiro (1961) Solar, Geomanetic, and Meteorological Periodicities. *Annals of the New York Academy of Sciences,* 95**,** 200-224.

Weedon, G. P. 2003. *Time-Series Analysis and Cyclostraigraphy: Examining Stratigraphic Records of Environmental Cycles*. New York: Cambridge University Press.

Winslow, A. (1893) The Osage River and its Meanders. *Science (New York, N.Y.),* 22**,** 31-2.

Yoo, H. 2001. 2D Continuous Wavelet Transform.

Zhang, Y., Z. Dong, L. Wu & S. Wang (2011) A hybrid method for MRI brain image classification. *Expert Systems with Applications,* 38**,** 10049-10053.

Zolezzi, G. & I. Güneralp (2016) Continuous wavelet characterization of the wavelengths and regularity of meandering rivers. *Geomorphology,* In print.